Behavioral/Systems/Cognitive

Sodium Channel $Na_v1.7$ Is Essential for Lowering Heat Pain Threshold after Burn Injury

Shannon D. Shields,[1,2] Xiaoyang Cheng,[1,2] Nurcan Üçeyler,[3] Claudia Sommer,[3] Sulayman D. Dib-Hajj,[1,2] and Stephen G. Waxman[1,2]

[1]Department of Neurology and Center for Neuroscience and Regeneration Research, Yale University School of Medicine, New Haven, Connecticut 06520, [2]Rehabilitation Research Center, Veterans Affairs Connecticut Healthcare System, West Haven, Connecticut 06516, and [3]Department of Neurology, University of Würzberg, 97080 Würzberg, Germany

Marked hypersensitivity to heat and mechanical (pressure) stimuli develop after a burn injury, but the neural mechanisms underlying these effects are poorly understood. In this study, we establish a new mouse model of focal second-degree burn injury to investigate the molecular and cellular basis for burn injury-induced pain. This model features robust injury-induced behavioral effects and tissue-specific altered cytokine profile, but absence of glial activation in spinal dorsal horn. Three voltage-gated sodium channels, $Na_v1.7$, $Na_v1.8$, and $Na_v1.9$, are preferentially expressed in peripheral somatosensory neurons of the dorsal root ganglia (DRGs) and have been implicated in injury-induced neuronal hyperexcitability. Using knock-out mice, we provide evidence that $Na_v1.7$ selectively contributes to burn-induced hypersensitivity to heat, but not mechanical, stimuli. After burn model injury, wild-type mice display increased sensitivity to heat stimuli, and a normally non-noxious warm stimulus induces activity-dependent Fos expression in spinal dorsal horn neurons. Strikingly, both effects are absent in $Na_v1.7$ conditional knock-out (cKO) mice. Furthermore, burn injury increases density and shifts activation of tetrodotoxin-sensitive currents in a hyperpolarized direction, both pro-excitatory properties, in DRG neurons from wild-type but not $Na_v1.7$ cKO mice. We propose that, in sensory neurons damaged by burn injury to the hindpaw, $Na_v1.7$ currents contribute to the hyperexcitability of sensory neurons, their communication with postsynaptic spinal pain pathways, and behavioral thresholds to heat stimuli. Our results offer insights into the molecular and cellular mechanisms of modality-specific pain signaling, and suggest $Na_v1.7$-blocking drugs may be effective in burn patients.

Introduction

Pain induced by burn injury is typified by a spontaneous ongoing unpleasant sensation, as well as persistent hypersensitivity to heat and mechanical (pressure) stimuli. Despite the common occurrence of burn injury-induced pain, very little is known about its neural underpinnings. Globally, 11 million people per year suffer burns severe enough to require medical attention (Peck, 2011), underscoring the important need for effective treatments for burn injury-related pain. Against this background, it is striking that the basic mechanisms of burn injury-related pain have been relatively understudied in preclinical animal models.

Received Jan. 20, 2012; revised May 10, 2012; accepted June 15, 2012.

Author contributions: S.D.S., N.Ü., S.D.D.-H., and S.G.W. designed research; S.D.S., X.C., and N.Ü. performed research; S.D.S., X.C., N.Ü., C.S., S.D.D.-H., and S.G.W. analyzed data; S.D.S., X.C., N.Ü., S.D.D.-H., and S.G.W. wrote the paper.

This work was supported by the Medical Research Service and Rehabilitation Research Service of the Department of Veterans Affairs and by intramural funds from the University of Würzburg, Germany. The Center for Neuroscience and Regeneration Research is a collaboration of the Paralyzed Veterans of America and the United Spinal Association with Yale University. We gratefully acknowledge Professor John Wood for the generous gift of breeding stock for the $Na_v1.7$, $Na_v1.8$, and $Na_v1.9$ mutant mouse colonies; the excellent technical assistance of Pam Zwinger, Lawrence Macala, Peng Zhao, Palak Shah, and Sonja Mildner; and Grégory Scherrer for helpful comments on the manuscript.

Correspondence should be addressed to Stephen G. Waxman, Neuroscience and Regeneration Research Center, Veterans Affairs Connecticut Healthcare System, 950 Campbell Avenue, Building 34, West Haven, CT 06516. E-mail: stephen.waxman@yale.edu.

DOI:10.1523/JNEUROSCI.0304-12.2012

 0270-6474/12/3210819-14$15.00/0

Three voltage-gated sodium channels (VGSCs), $Na_v1.7$, $Na_v1.8$, and $Na_v1.9$, are preferentially expressed in primary somatosensory afferents specialized to sense noxious stimuli (nociceptors). These three channels have partially overlapping expression patterns, and are responsible for different aspects of electrogenesis and action potential propagation within sensory neurons of the dorsal root ganglia (DRGs) (Black et al., 1996; Cummins and Waxman, 1997; Tate et al., 1998; Cummins et al., 1999; Amaya et al., 2000; Renganathan et al., 2001; Blair and Bean, 2002; Pinto et al., 2008). Several groups have studied the contributions of $Na_v1.7$, $Na_v1.8$, and $Na_v1.9$ to nociception using mutant mouse models. Generally, these studies found little to no change in acute nociceptive thresholds and mild deficits in inflammation-induced hypersensitivity in mice lacking $Na_v1.8$ or $Na_v1.9$ (Akopian et al., 1999; Kerr et al., 2001; Priest et al., 2005; Amaya et al., 2006; Leo et al., 2010). On the other hand, a single study reported a large reduction in hypersensitivity induced by various inflammogens in $Na_v1.7$ conditional knock-out (cKO) mice, in which $Na_v1.7$ was deleted from a subset of sensory neurons (Nassar et al., 2004). Whether burn injury-induced pain shares common mechanisms with models of inflammatory pain is not currently known.

Separate lines of evidence have implicated $Na_v1.7$ in the sensation of pain experienced by human subjects with inherited erythromelalgia, who harbor gain-of-function mutations in the *SCN9A* gene encoding for this sodium channel (Yang et al., 2004; Drenth and Waxman, 2007; Dib-Hajj et al., 2010). Thus, single

amino acid substitutions demonstrated to alter the biophysical gating properties of $Na_v1.7$ channels and to render DRG neurons hyperexcitable in culture manifest in these patients as a recurrent and debilitating pain syndrome triggered by exposure to warmth and usually described as "burning" (Cummins et al., 2004; Dib-Hajj et al., 2005, 2008; Han et al., 2006, 2009; Harty et al., 2006; Rush et al., 2006; Estacion et al., 2008; Lampert et al., 2008; Choi et al., 2010; Cheng et al., 2011). Whether $Na_v1.7$ contributes similarly to pain following burn injury has thus far remained unexplored.

In the present report, we establish a mouse model of focal second-degree burn injury and use it to investigate the individual contributions of $Na_v1.7$, $Na_v1.8$, and $Na_v1.9$ to injury-induced sensitization. We present evidence that $Na_v1.7$ is essential for burn-induced heat hypersensitivity. Our results offer new insights into the mechanisms of modality-specific pain signaling and suggest that $Na_v1.7$-blocking drugs currently under development may be effective in burn patients.

Materials and Methods

Animal experiments were approved by the Institutional Animal Care and Use Committee at the Veterans Administration Connecticut Healthcare System, and conducted in accordance with the National Institutes of Health Guide for the Care and Use of Laboratory Animals and the recommendations of the International Association for the Study of Pain.

Mice. Animals were housed 2–5 per cage and maintained on a 12 h light/dark schedule in a temperature-controlled environment with *ad libitum* access to food and tap water. Wild-type C57BL/6 mice purchased from Charles River were used for establishing the burn injury model (see Figs. 1–3). For experiments with mutant mice, we made comparisons between $Na_v1.7$ cKO [$Na_v1.8^{Cre/+}$; $Na_v1.7^{loxP/loxP}$] (Nassar et al., 2004) and control littermates [$Na_v1.8^{+/+}$; $Na_v1.7^{loxP/loxP}$], between $Na_v1.8$ KO [$Na_v1.8^{-/-}$] (Akopian et al., 1999) and wild-type littermates, or between $Na_v1.9$ KO [$Na_v1.9^{-/-}$] (Ostman et al., 2008) and wild-type littermates. $Na_v1.7$ cKO mice were used because $Na_v1.7$ global knock-out mice die perinatally (Nassar et al., 2004). To target the correct population of sensory neurons in our electrophysiology experiments, we additionally introduced a Cre-reporter gene to $Na_v1.7$ cKO mice by directed breeding with tdTomato Cre-reporter mice (B6.Cg-*Gt(ROSA)26Sor*$^{tm14(CAG-tdTomato)Hze}$/J; stock #007914) (Madisen et al., 2010) purchased from Jackson Laboratories. Mice used for electrophysiology experiments thus bore the genotypes [$Na_v1.8^{Cre/+}$; $Na_v1.7^{loxP/loxP}$; $Rosa26^{tdTomato/tdTomato}$] or [$Na_v1.8^{Cre/+}$; $Na_v1.7^{+/+}$; $Rosa26^{tdTomato/tdTomato}$]. Adult mice (8–20 weeks) of both sexes were used for all experiments. $Na_v1.7$ cKO, $Na_v1.8$ KO, and $Na_v1.9$ KO mice (and control littermates) were derived from breeding stock originally provided by Professor John Wood (University College London, UK) and bred at our facility in West Haven, Connecticut, for at least 11, 13, or 4 generations, respectively, maintained on a C57BL/6 background. PCR genotyping was performed as described previously for $Na_v1.7$ cKO and $Na_v1.9$ mutant mice (Nassar et al., 2004; Ostman et al., 2008), or using forward primers GCCTTCACTGTTGTTTACACCTTC GAGG (wild-type) and GCAGCGCATCGCCTTCTATC (knock-out) and the common reverse primer GAGTGATGCATATGATGTCATGTGTGG for $Na_v1.8$ mutant mice, or according to the The Jackson Laboratory website (http://jaxmice.jax.org/strain/007914.html) for tdTomato Cre-reporter mice.

Burn injury model. Methods for the burn injury model in mice were adapted from our group's previous work with rats (Chang et al., 2010). Anesthesia was induced with 2% isoflurane and maintained for 5 min before the procedure and continuously throughout the duration of the procedure. A hollow metal plate through which water circulated from a 65°C water bath was arranged on the bench. One hindpaw of each mouse was held in contact with the metal plate for 15 s. Mice were allowed to recover from anesthesia in their homecages immediately afterward. Sham-treated animals underwent identical treatment except that the hindpaw was held in contact with a room temperature metal plate.

Histology

Tissue preparation. Mice were deeply anesthetized with ketamine and xylazine (100 and 10 mg/kg, i.p.) and perfused transcardially with 0.1 M PBS followed by 4% paraformaldehyde in PBS. Spinal cords and DRGs were collected, postfixed in the same fixative for 4 h, and cryoprotected overnight in 0.1 M PBS containing 30% sucrose. Using a cryostat, spinal cords were cut at 30 μm and processed as free-floating sections, and DRGs were cut at 14 μm and processed on slides.

Immunohistochemistry. Immunohistochemistry was performed as described previously (Shields et al., 2007). Primary antisera were as follows: rabbit anti-Iba-1 (1:250; Wako Chemicals); mouse anti-glial fibrillary acidic protein (GFAP) (1:2000; Millipore Bioscience Research Reagents/Millipore); rabbit anti-activating transcription factor (ATF)-3 (1:200; Santa Cruz Biotechnology); sheep anti-calcitonin gene-related (CGRP) peptide (1:2000; Abcam); or a mixture of chicken anti-neurofilament (NF)-H, chicken anti-NF-M, and chicken anti-NF-L (all 1:1000; EnCor Biotechnology). Secondary antisera were species-appropriate biotinylated (1:200; Vector Laboratories) or fluorophore-conjugated antibodies made in donkey (1:1000; Invitrogen). When appropriate, biotinylated IB4 (1:500; Sigma) and Alexa 488-conjugated streptavidin (1:1000; Invitrogen) were added in place of primary and secondary antibodies.

Image analysis. Images were captured using either a Nikon E800 microscope for bright-field images or a Nikon E600 confocal microscope for fluorescent images. Image analysis was performed using ImageJ software (http://rsbweb.nih.gov/ij). For DRG neuron colocalization counting and area measurements, data were collected from at least three sections per animal from at least three animals. Two perpendicular diameters were measured from each neuron with a clearly visible nucleus in the tissue section, and the cell's area (in μm^2) was calculated: area = $(d_1/2)^*(d_2/2)^*\pi$. Each neuron was scored for the presence or absence of ATF-3 labeling and the molecular markers of DRG neuron classes. For densitometry measurements in spinal cord sections, the dorsal horn gray matter on one side of the spinal cord was outlined, and pixel density and measurement area were recorded. The same outline was then reflected horizontally and fitted to the analogous region on the other side of the spinal cord, where the measurements were again recorded. Background, measured in a region selected from adjacent gray matter on each side, was subtracted from each pixel density measurement. Densitometry analysis was done by an experimenter blinded to the treatment group of the animal and the side (ipsilateral vs contralateral) of treatment.

Cytokine measurements

Tissue collection. Twenty-four hours after burn injury mice were deeply anesthetized with a mixture of ketamine and xylazine (100 and 10 mg/kg, i.p.) and killed by decapitation. The following tissue was dissected and immediately flash-frozen in liquid nitrogen for quantitative real-time PCR (qRT-PCR) studies: skin of the plantar surface of the hindpaws, sciatic nerve, L4–L6 DRG, lumbar spinal cord, and thalamus. Except for the control animals, tissue from the ipsilateral and contralateral sides was collected separately. Tissue was stored at −80°C before further processing.

mRNA extraction. For mRNA extraction from mouse hindpaw skin, frozen tissue was homogenized on ice using an Ultraturrax homogenizer (Polytron PT 1600E; Kinematica). Thereafter the RNeasy Mini Kit (Qiagen) was used for mRNA extraction following the manufacturer's instructions.

mRNA extraction from mouse nervous tissue was performed following the method of Chomczynski and Sacchi (1987) with slight modification as described previously (Uçeyler et al., 2007). Frozen tissue was incubated in TRIzol reagent (Invitrogen) and was homogenized. Chloroform was added and the samples were centrifuged (13,000 *g* for 15 min at 4°C). The upper phase was mixed with glycogen and propanol and after overnight incubation at −20°C the samples were washed with 75% ethanol. Extracted mRNA was dissolved in diethylpyrocarbonate-treated water. The mRNA yield was quantified photometrically (Eppendorf) and the 260/280 ratio was measured for determining the integrity of the extracted RNA.

Reverse transcription PCR. PCR reagents and cyclers were obtained from Applied Biosystems. For reverse transcription PCR TaqMan Reverse Transcription Reagents were used. A reaction of 100 μl contained

500 ng of mRNA and the following reagents (per sample): 10× Reaction Buffer (10 μl), 10 mM dNTPs (20 μl), 25 mM $MgCl_2$ (22 μl), Random Hexamers (5 μl), RNase Inhibitor (2 μl), and 50 U/μl Multiscribe Reverse Transcriptase (6.25 μl). The 96-well GeneAmp PCR System 9700 cycler was used for the reaction. The cycler conditions were as follows: 10 min, 38°C; 60 min, 48°C; and 25 min, 95°C.

qRT-PCR. We investigated the relative gene expression of the following markers (Applied Biosystems Assay-ID in parentheses): pro-inflammatory cytokines tumor necrosis factor (TNF) (Mm00443258_m1), interleukin (IL)-1β (Mm00434228_m1), and IL-6 (Mm99999064_m1); the anti-inflammatory cytokine IL-10 (Mm00439616_m1); and the chemokine CXCL5 (Mm00436451_g1). Then 18sRNA was measured as housekeeping gene to normalize the values. Five microliters of cDNA was taken for qRT-PCR, which was performed in the StepOnePlus Real Time PCR System capable of fluorescence measurement using TaqMan Universal Master Mix as previously described (Uçeyler et al., 2007).

Behavioral testing

Mice were habituated to the test apparatus for at least 60 min before testing on each test day. After behavioral testing was completed on each test day, paw diameter was measured using a spring-loaded caliper (Mitutoyo). Behavioral testing was performed blind to treatment group.

Hindpaw radiant heat (Hargreaves') test. Mice were placed in plastic chambers on a glass surface maintained at 25°C. A radiant heat source (University of California San Diego Anesthesiology Department, La Jolla, CA) was focused on the hindpaw and latency to respond was recorded in three trials per paw, separated by at least 10 min. Cutoff to avoid tissue damage was 20 s.

von Frey test of mechanical threshold. Mice were placed in plastic chambers on a wire mesh grid and stimulated with von Frey filaments (Stoelting) according to the up-down method of Chaplan et al. (1994).

Fos induction

Experiments were performed largely as described previously (Cavanaugh et al., 2009) on day 7 after burn injury or sham procedure. One group of mice was deeply anesthetized with urethane (1.5 g/kg) continuously throughout the experiment, and received a warm stimulus, consisting of immersion of the affected hindpaw in a 40°C water bath three times for 30 s each, with a 30 s interval between stimuli. Survival time between stimulus and perfusion/tissue collection was 90 min. Nonstimulated control mice received identical anesthesia and timing, but no paw immersion. A second group of mice walked on a Rotarod apparatus (Accuscan Instruments) at a speed of 5 rpm continuously for 90 min, then rested in their cages for an additional 30 min before perfusion/tissue collection (Jasmin et al., 1994; Neumann et al., 2008). After spinal cord removal and sectioning as described above, immunohistochemistry was performed using rabbit anti-Fos primary antibody (1:5000; Abcam), biotinylated donkey anti-rabbit secondary antibody (1:200; Vector Laboratories), Extravidin-peroxidase (1:1500; Sigma), and 3,3′-diaminobenzidine (Sigma) as chromogen. Fos-positive profiles were counted from 8 to 10 sections per animal from at least three animals per group, using dark-field microscopy to differentiate between laminae II and III, as described previously (Cavanaugh et al., 2009).

Primary DRG culture

DRG neurons were isolated from the ipsilateral L4–L6 ganglia of four 30-week-old mice that had undergone burn model injury or sham treatment 2 d earlier. Electrophysiological recordings or calcium imaging experiments were performed the following day (3 d after burn or sham). The neurons were isolated as previously described (Dib-Hajj et al., 2009) with the exceptions that Liberase Blendzyme 4 was replaced with Liberase TM Research Grade and Liberase Blendzyme 3 was replaced with Liberase TL Research Grade. Briefly, after dissection, the tissue was incubated for 20 min at 37°C in oxygenated complete saline solution (CSS; 137 mM NaCl, 5.3 mM KCl, 1 mM $MgCl_2$, 25 mM sorbitol, 10 mM HEPES, and 3 mM $CaCl_2$, pH 7.2) containing 0.5 U/ml Liberase TM (Roche Diagnostics) and 0.6 mM EDTA. This solution was then centrifuged (100 *g* for 3 min); exchanged with oxygenated CSS containing 0.5 U/ml Liberase TL (Roche), 0.6 mM EDTA, and 30 U/ml papain (Worthington Biochemical); and incubated at 37°C for 15 min. After incubation the ganglia were centrifuged (100 *g* for 3 min), and then triturated in DRG media [DMEM/F12 (1:1) supplemented with 100 U/ml penicillin, 0.1 mg/ml streptomycin (Invitrogen) and 10% fetal calf serum (Hyclone)] containing 1.5 mg/ml bovine serum albumin (low endotoxin) and 1.5 mg/ml trypsin inhibitor (Sigma). Cells were then plated on 12 mm poly-D-lysine/laminin-coated glass coverslips (BD Biosciences) for electrophysiology experiments or on 35 mm poly-D-lysine-coated glass-bottom culture dishes (MatTek) for calcium imaging experiments and incubated at 37°C in a 95% air/5% CO_2 incubator. After 30 min DRG media (1 ml/well) was added. No growth factors were added to the media.

Voltage-clamp electrophysiology

Small (20–25 μm) DRG neurons were used for voltage-clamp recording within 12–36 h in culture. Electrodes had a resistance of 1–2 MΩ when filled with the pipette solution, which contained the following (in mM): 140 CsF, 10 NaCl, 1 EGTA, 10 dextrose, and 10 HEPES, pH 7.30 (adjusted with CsOH), and the osmolarity was adjusted to 315 mOsmol/L with sucrose. The extracellular bath solution contained the following (in mM): 70 NaCl, 70 choline chloride, 3 KCl, 1 $MgCl_2$, 1 $CaCl_2$, 20 TEACl, 5 CsCl, 0.1 $CdCl_2$, and 10 HEPES, pH 7.30 (adjusted with NaOH), and the osmolarity was 328 mOsmol/L. The whole-cell recording configuration was obtained in voltage-clamp mode with an Axopatch 200B amplifier (Molecular Devices). Data were collected via a Digidata 1322a A/D converter (Molecular Devices) at 50 kHz and filtered at 5 kHz. Voltage errors were minimized with 80–90% series resistance compensation, and linear leak currents and capacitance artifacts were subtracted out using the P/6 method. The amplitude of tetrodotoxin-sensitive (TTX-S) sodium channels was estimated via two activation protocols as previously described (Rush et al., 2005). The first protocol was recorded at 5 min after forming whole-cell configuration. Cells were held at −80 mV, a 500 ms depolarizing prepulse (−50 mV) was applied to inactivate the majority of TTX-S sodium channels, and voltage-dependent inward currents, mainly generated through $Na_v1.8$ channels, were initiated with a series of step depolarizations from −80 to +50 mV (in 5 mV increments). Cells exhibiting $Na_v1.9$ currents were excluded from data analysis. The second protocol was started at 10 min after forming whole-cell configuration. Cells were held at −80 mV, a 500 ms hyperpolarizing prepulse (−120 mV) was applied to rescue the majority of TTX-S channels from inactivation, and total sodium currents were evoked by a series of depolarizing steps from −80 to +50 mV (in 5 mV increments). An estimate of TTX-S currents was obtained by subtraction of the currents obtained from the two protocols using Clampfit 9.2 (Molecular Devices).

Activation curves were obtained by converting current (I) to conductance (G) at each voltage (V) using the equation $G = I/(V - V_{rev})$. Activation curves were fit with Boltzmann functions as follows:

$$G = \frac{G_{max}}{1 + e^{\frac{V_{1/2,act} - V}{k}}},$$

where G_{max} is maximal sodium conductance, $V_{1/2,act}$ is the potential of half-maximal activation, V is the test potential, and k is the slope factor.

For steady-state fast inactivation, cells were held at −100 mV. Steady-state fast inactivation was achieved with a series of 500 ms prepulses (−140 to −10 mV in 10 mV increments) and the remaining noninactivated channels were activated by a 40 ms step depolarization to −10 mV. Peak inward currents were normalized to the maximal peak current (I_{max}).

Cells producing a large fraction of $Na_v1.8$ currents exhibit two phases of fast inactivation, with TTX-S channels contributing to the first inactivation phase and $Na_v1.8$ channels contributing to the second inactivation phase, and were fit with a double Boltzmann function as follows:

$$I/I_{max} = Y_0 + A\left(\frac{frac}{1 + e^{\frac{V - V_{1/2,fast1}}{k_1}}} + \frac{1 - frac}{1 + e^{\frac{V - V_{1/2,fast2}}{k_2}}}\right),$$

where y_0 represents the fraction of channels resistant to fast inactivation, A represents the fraction of inactivated channels, *frac* represents the percentage of inactivation caused by TTX-S channels, (1-*frac*) represents the percentage of inactivation caused by $Na_v1.8$ channels, and $V_{1/2,fast1}$ and $V_{1/2,fast2}$ represent the inactivation midpoints of TTX-S channels and $Na_v1.8$ channels, respectively.

Cells producing small $Na_v1.8$ currents or cells unable to be fit by double Boltzmann functions were fit with single Boltzmann functions as follows:

$$I/I_{max} = A + \frac{1 - A}{1 + e^{\frac{V - V_{1/2,fast}}{k}}},$$

where V represents the inactivating prepulse potential and $V_{1/2,fast}$ represents the inactivation midpoint.

Calcium imaging

Cells were loaded with 2 μM Fura-2-AM (Invitrogen) in standard bath solution (SBS; 140 mM NaCl, 3 mM KCl, 1 mM $MgCl_2$, 1 mM $CaCl_2$, and 10 mM HEPES, pH 7.3, 320 mOsm) with 0.02% Pluronic F-127 (Invitrogen) at room temperature for 30 min, then washed in SBS and allowed to incubate in 1.5 ml SBS for a further 10 min. Cells from a single field per dish were imaged using a Nikon Ti-E inverted microscope and illuminated using a fast-switching xenon light source (Lambda DG-4; Sutter Instruments) for 500 ms, alternately at 340 and 380 nm. Images were captured with a QuantEM CCD camera (Princeton Instruments), and digitized, background corrected, and analyzed with NIS-Elements software (Nikon). Background-corrected 340/380 ratio images were collected every 2 s during the experiment. Cells were stimulated with heated SBS and with high potassium solution (SBS with 75 mM KCl). For heat stimulation, 4.5 ml of SBS at 75°C was applied to cells in 1.5 ml SBS at 22°C. A small thermoprobe (AutoMate Scientific) located in the culture dish allowed us to determine that, under our experimental conditions, cells were transiently exposed to a peak temperature of 46.7 ± 0.3 and 46.6 ± 0.7°C for the sham and burn groups, respectively. In general, the temperature reached a peak within ~20 s of application of heated SBS, perfusion of room temperature SBS as a washout step was begun at 80 s after applying the heat pulse, and application of high potassium SBS occurred at the end of the experiment. Each culture dish was thus subject to a single exposure to the heat stimulus. All neurons that responded to high potassium SBS were included for analysis. A positive heat response was assigned to a neuron if its 340/380 ratio during stimulus application reached at least 20% of the maximal 340/380 ratio it achieved during stimulation with 75 mM KCl. Neurons were cultured from three mice per group.

Statistical analysis

For statistical analysis, SPSS software or OriginPro8.1 (Microcal Software) was used. The qRT-PCR data showed non-normal distribution in the Kolmogorov–Smirnov test; therefore we used the nonparametric Mann–Whitney U test. Behavioral, electrophysiology, and densitometry data were analyzed using Student's unpaired t test or repeated-measures ANOVA when normally distributed; otherwise the Mann–Whitney U test or Friedman's statistic was used. In all cases, statistical significance was assumed at $p < 0.05$.

Results

A new mouse model of burn injury-induced pain

To study the molecular and cellular bases for burn injury-induced sensitization, we first established a model of focal second-degree burn in mice. Deeply anesthetized mice underwent contact of a single hindpaw for 15 s with a metal plate held at 65°C (burn injury model) or at room temperature (sham procedure). We found this protocol to reliably produce reduced withdrawal thresholds to heat and mechanical stimuli in the affected hindpaw that were present at the earliest time point examined (2–4 h after the procedure) and lasted 2–3 weeks (Fig. 1*A*, *C*). No changes in response thresholds were noted in sham-treated animals or in the contralateral hindpaw of burn model animals (Fig. 1*A–D*). The burn model was also associated with prominent edema of the affected hindpaw that resolved with a similar time course to the sensory changes (Fig. 1*E*). In pilot studies using other temperatures (75°C or 85°C) to produce the burn injury, we observed changes in response thresholds to heat and mechanical stimuli that did not differ significantly in magnitude or duration from those found in the 65°C model, although more damage to the skin and digits was present (data not shown). Therefore we favor the 65°C burn model in the mouse. Based on our sensory testing results, we considered that peak behavioral hypersensitivity occurred between 3 and 7 d after burn injury, so this time window was used in subsequent experiments for characterizing the model and exploring mechanisms of burn injury-induced pain. Because this model recapitulates several of the features of burn injury in humans, including edema and focal hypersensitivity to both heat and mechanical stimuli that eventually resolve as the burn heals, we present it as a new mouse model for use in preclinical research into the mechanisms and treatment of burn injury-induced pain.

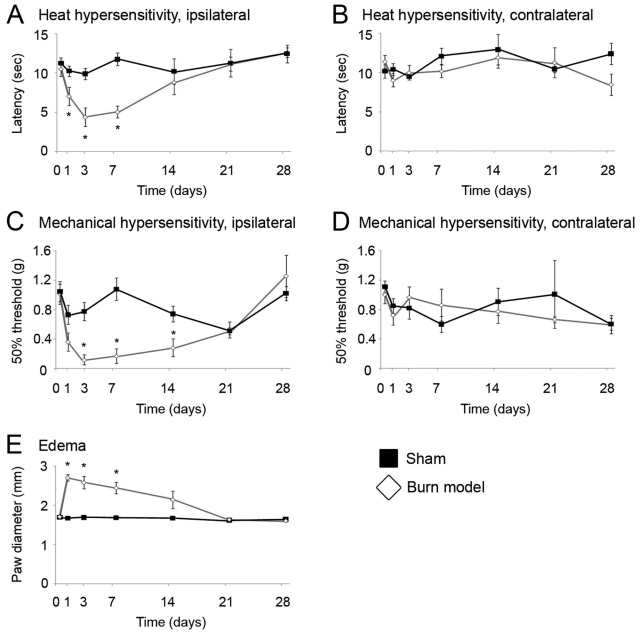

Figure 1. A mouse model of burn injury-induced pain produces peripheral edema and focal hypersensitivity to heat and mechanical stimuli. ***A***, Response thresholds to radiant heat stimuli (Hargreaves' test) are strongly decreased on the ipsilateral side in burn model animals and unchanged in sham-treated animals. Heat hypersensitivity is present at the earliest time point assessed and resolves within 2 weeks. (Repeated-measures ANOVA, $p < 0.05$; $n = 12$ mice/group.) ***B***, In the contralateral hindpaw, no significant difference in response threshold to the heat stimulus was noted between burn model and sham-treated animals at any time point. ***C***, Response thresholds to mechanical stimuli in the von Frey test are strongly decreased on the ipsilateral side in burn model animals and unchanged in sham-treated animals. Mechanical hypersensitivity resolves within 3 weeks. (Repeated-measures ANOVA, $p < 0.05$; $n = 12$ mice/group.) ***D***, In the contralateral hindpaw, no significant difference in response threshold to the mechanical stimuli was noted between burn model and sham-treated animals at any time point. ***E***, A prominent edema develops in burn model animals, as measured by an increased paw diameter. Paw swelling is resolved within ~2 weeks of burn injury in this model. (Repeated-measures ANOVA, $p < 0.05$; $n = 12$ mice/group.) *$p < 0.05$.

The mouse burn model incorporates some features of both inflammatory and neuropathic pain states

To characterize the sequelae of burn injury in our model, we examined three types of injury-induced changes: induction of ATF-3 in DRG neurons, gliosis in the spinal cord, and cytokine gene regulation.

The nerve injury marker ATF-3 is induced in DRG neurons after burn injury of the hindpaw

Sensory and motor neurons that are directly injured, for example, by peripheral axotomy, begin to express the transcription factor

Table 1. ATF-3, a transcription factor induced in injured neurons, is expressed in L4–L6 DRG neurons after hindpaw heat injury

	% Total	% ATF-3	% CGRP	% IB4	% NF
L4 DRG					
ATF-3	8.9 ± 1.4	—	4.8 ± 2.4	1.7 ± 0.8	6.8 ± 3.1
CGRP	28.1 ± 3.9	9.2 ± 4.7	—	N/D	N/D
IB4	34.3 ± 4.0	6.7 ± 3.4	N/D	—	N/D
NF	32.3 ± 5.1	21.1 ± 3.7	N/D	N/D	—
L5 DRG					
ATF-3	25.5 ± 1.6	—	14.2 ± 5.5	20.8 ± 5.6	26.2 ± 5.7
CGRP	29.1 ± 1.3	15.3 ± 4.7	—	N/D	N/D
IB4	32.3 ± 2.0	25.8 ± 6.3	N/D	—	N/D
NF	34.9 ± 1.8	35.2 ± 3.5	N/D	N/D	—
L6 DRG					
ATF-3	4.5 ± 2.0	—	2.7 ± 2.7	5.8 ± 3.7	0.0 ± 0.0
CGRP	31.1 ± 3.7	5.5 ± 5.5	—	N/D	N/D
IB4	35.2 ± 6.0	25.0 ± 4.8	N/D	—	N/D
NF	30.7 ± 3.1	0.0 ± 0.0	N/D	N/D	—

Note that all types of sensory neurons are affected, without bias for neurochemical type, in a topographical (segmental) pattern corresponding to total contribution to the innervation of the plantar surface of the hindpaw. CGRP, calcitonin gene-related peptide; NF, neurofilament.

ATF-3, and expression of this protein has come to be widely regarded as a marker for nerve injury (Tsujino et al., 2000; Tsuzuki et al., 2001; Seijffers et al., 2006; Peters et al., 2007; Bráz and Basbaum, 2009). We asked whether sensory neurons are directly injured in our hindpaw burn model by performing immunohistochemistry for ATF-3 in the DRGs that contain cell bodies of sensory neurons that innervate the hindpaw (lumbar segments L4–L6). Approximately 10, 25, and 5% of total neurons in the ipsilateral L4, L5, and L6 DRGs, respectively, express ATF-3 1 week after burn injury (Table 1; Fig. 2). ATF-3-positive DRG neurons span all size categories (Fig. 2), and there does not appear to be a particular bias for ATF-3 to be induced in neurons of any specific neurochemical type (Table 1). Rather, it appears that ATF-3 is present in a representative set of sensory neurons in each ganglion, approximately in proportion to that ganglion's contribution to the innervation of the plantar surface of the hindpaw (Devor et al., 1985; Swett et al., 1991; Takahashi et al., 1994). These observations provide evidence that some DRG neurons are directly injured in the burn model.

Furthermore, we asked whether cultured DRG neurons derived from mice with hindpaw burn injury are hypersensitive to heat stimuli *in vitro*. Using a calcium imaging assay, we found that 48.7 ± 1.5% of L4–L6 DRG neurons derived from sham-treated mice responded to application of heated buffer ($n = 3$ mice, 258 neurons). The incidence of heat responsiveness we observed in these control conditions is similar to that reported by several other groups using a variety of *in vitro* techniques (Cesare and McNaughton, 1996; Nagy and Rang, 1999; Caterina et al., 2000). In contrast, 78.2 ± 7.4% of L4–L6 DRG neurons from mice that had undergone burn model injury were heat responsive under the same conditions ($p = 0.0179$, $n = 3$ mice, 539 neurons). These results establish that DRG neurons derived from mice with hindpaw burn injury are measurably hypersensitive, *in vitro*, to heat stimuli in the noxious range.

Microgliosis and astrocytosis are absent in lumbar spinal cord after burn injury of the hindpaw

Changes in spinal cord glia provide an important contribution to persistent hypersensitivity in nerve injury-induced neuropathic pain. Microglia, and to a lesser extent astrocytes, are present in greater numbers and display a hypertrophic, "reactive" morphology after injury to a peripheral nerve (Tsuda et al., 2003, 2005; Coull et al., 2005; Narita et al., 2006; Scholz and Woolf, 2007; Thacker et al., 2009; Ren, 2010). Such changes are not generally reported in models of inflammatory pain (Sweitzer et al., 1999; Ledeboer et al., 2006; Ren and Dubner, 2010).

We compared reactive microglial Iba-1 staining (Polgár et al., 2005; Narita et al., 2006) in sham-treated versus burn model animals at several time points. As a positive control, we stained lumbar spinal cord from mice that had undergone sciatic axotomy 1 week before. As expected, we observed a large increase in Iba-1 microglial staining in the ipsilateral dorsal horn and motor neuron pools from axotomized mice (dorsal horn, 335 ± 30% of sham, $p < 0.001$). However, no significant microglial changes compared with sham-treated animals were noted after burn model injury any of the time points examined (1, 7, 14, and 28 d; data not shown). Similarly, we found no evidence for astrocytosis in burn model animals at these time points, measured by GFAP labeling (data not shown).

Pro- and anti-inflammatory cytokines are differentially regulated along the pain–sensory neuraxis after burn injury of the hindpaw

Differential gene regulation of multiple pro- and anti-inflammatory cytokines is a feature of several injury-associated pain models, and several cytokines have been identified as potential pain biomarkers or targets for analgesic drugs (White et al., 2007; Uçeyler and Sommer, 2008; Abbadie et al., 2009). In addition, one member of this family, CXCL5, has recently been implicated in pain-like behaviors in a sunburn model (Dawes et al., 2011). We determined the cytokine profile of multiple tissues along the pain–sensory neuraxis in mice 24 h after burn model injury, since changes in cytokine gene expression have been reported to occur with rapid onset in other pain models (Kleinschnitz et al., 2004; Uçeyler et al., 2007) and hypersensitivity in the burn injury model is already present at this time (Fig. 1).

Twenty-four hours after burn injury, gene expression of the pro-inflammatory cytokines TNF, IL-1β, and IL-6, and of the anti-inflammatory cytokine IL-10 increased in skin of the ipsilateral hindpaw ($p < 0.01$ for each) compared with tissue from naive or sham-treated animals. Expression of these target genes did not change on the contralateral side (Fig. 3*A*). We could not consistently detect CXCL5 in hindpaw skin from naive mice or from mice that had undergone burn model injury.

In the sciatic nerve, gene expression of the pro-inflammatory cytokines TNF ($p < 0.01$), IL-1β ($p < 0.001$), and of the anti-inflammatory cytokine IL-10 ($p < 0.01$) were increased ipsilaterally 24 h after burn injury. No changes were found for IL-6 or CXCL5 and again no changes were found for gene expression on the contralateral side (Fig. 3*B*; data not shown).

In L4–L6 DRG, burn model injury induced only an increase of the ipsilateral gene expression of IL-6 ($p < 0.01$), while no changes were found for the other cytokines (Fig. 3*C*).

In lumbar spinal cord, gene expression of TNF, IL-1β, and CXCL5 did not change 24 h after burn injury; however, gene expression of IL-6 ($p < 0.001$) and IL-10 ($p < 0.05$) decreased in the contralateral part of the lumbar spinal cord (Fig. 3*D*). This finding replicates similar decreases in cytokine gene expression reported in the CNS of mice in the chronic constriction injury model of neuropathic pain (Uçeyler et al., 2008). Gene expression of the investigated pro- and anti-inflammatory cytokines did not change in the ipsilateral or contralateral thalamus (Fig. 3*E*).

Together, our cytokine gene expression data map the profile of commonly regulated cytokines after burn injury, and indicate that CXCL5 upregulation may be unique to sunburn. The differential regulation of cytokines in the setting of burn injury indicates that the burn model possesses inflammatory-like qualities.

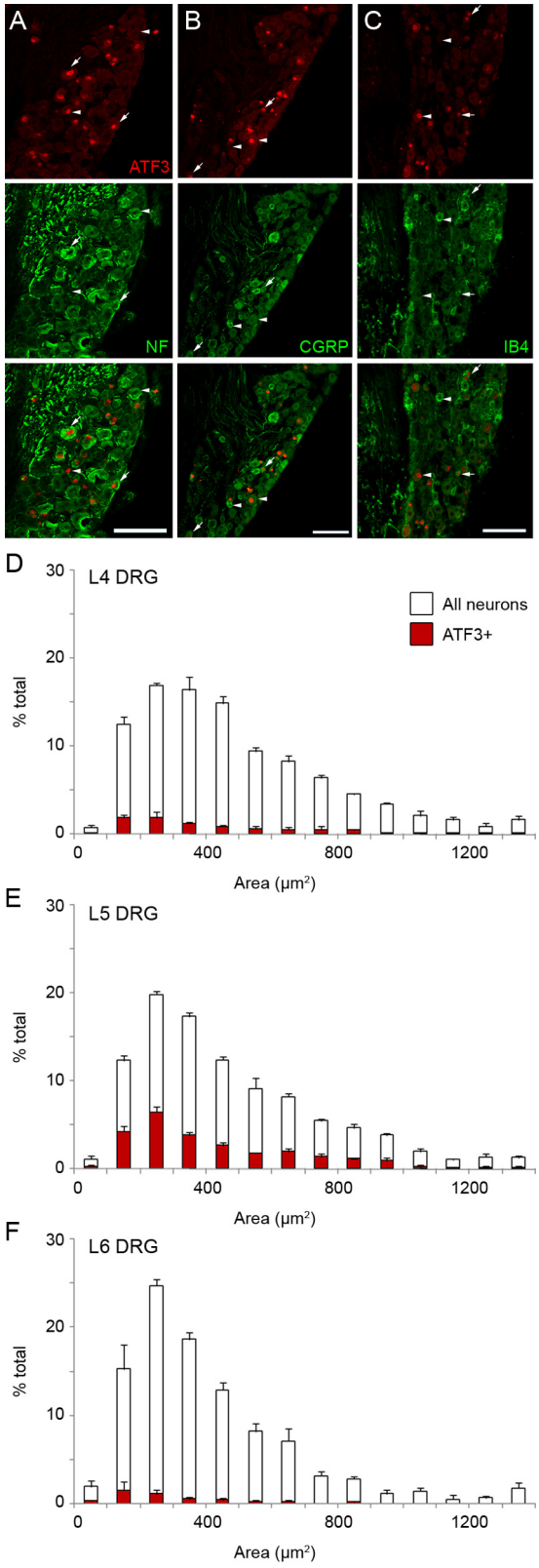

Figure 2. The nerve injury-related transcription factor ATF-3 is induced in DRG neurons after burn injury to the hindpaw. ATF-3 (***A–C***, red, top) is expressed in some DRG neurons after burn injury to the hindpaw, including those that express markers of various subtypes of sensory neurons (***A–C***, green, middle). The bottom image in each panel (***A–C***) is a merged view. Arrows highlight double-labeled neurons; arrowheads indicate single-labeled neurons. Scale bars, 100 μm. ***A***, Some ATF-3-positive cells express NF, a marker of neurons with myelinated axons (Aβ and Aδ afferents). ***B***, Some ATF-3-positive cells express CGRP, a marker that labels peptidergic C-nociceptors and some A-fiber afferents. ***C***, Some ATF-3-positive cells bind IB4, a marker of nonpeptidergic C-nociceptors. ***D–F***, Size distribution of sensory neurons in which ATF-3 is induced after hindpaw heat injury in lumbar DRGs L4 (***D***), L5 (***E***), and L6 (***F***). Quantification is provided in Table 1.

Sodium channel $Na_v1.7$ is necessary for heat but not mechanical hypersensitivity after burn injury

Having established and characterized our mouse burn model, we went on to employ this model to test our hypothesis that peripheral sodium channel isoforms may contribute differentially to burn injury-induced pain behaviors. In DRG neurons in which they are expressed, $Na_v1.7$ is thought to be activated by and to amplify small depolarizations such as those generated by primary transducer molecules, $Na_v1.8$ is thought to carry the bulk of the inward current underlying action potential upstroke, and $Na_v1.9$ may prolong subthreshold depolarizations (Cummins et al., 1998; Herzog et al., 2001; Renganathan et al., 2001; Blair and Bean, 2002; Rush et al., 2007). In these experiments, we tested mice in which $Na_v1.7$ is deleted from those sensory neurons that express $Na_v1.8$ ($Na_v1.7$ cKO; [$Na_v1.8^{Cre/+}$; $Na_v1.7^{loxP/loxP}$]) (Nassar et al., 2004), mice lacking $Na_v1.8$ ($Na_v1.8$ KO; [$Na_v1.8^{-/-}$]) (Akopian et al., 1999), and mice lacking $Na_v1.9$ ($Na_v1.9$ KO; [$Na_v1.9^{-/-}$]) (Ostman et al., 2008), each compared with their respective control littermates.

$Na_v1.7$ cKO mice do not differ from control mice in their response latencies at baseline (Fig. 4*A*,*B*). Strikingly, we found that $Na_v1.7$ cKO mice display a total lack of hypersensitivity to heat stimuli after burn model injury (Fig. 4*A*). Rather, their withdrawal thresholds to heat stimuli remain stable (Fig. 4*A*) despite the injury and prominent edema (data not shown). On the other hand, these mice develop robust mechanical hypersensitivity, comparable to control mice (Fig. 4*A*). $Na_v1.8$ KO and $Na_v1.9$ KO mice are indistinguishable from control mice in their behavioral responses to heat and mechanical stimuli both before and after burn model injury (Fig. 4*A*).

To determine whether this phenotype is restricted to our burn injury model or if it might be generalizable to other inflammatory pain models, we repeated testing on separate cohorts of mice using the complete Freund's adjuvant (CFA) model of inflammatory pain. Again, $Na_v1.7$ cKO mice failed to develop heat hypersensitivity in the CFA model, while mechanical hypersensitivity developed normally (Fig. 4*B*). $Na_v1.8$ KO and $Na_v1.9$ KO mice do not display significant differences from wild-type mice in their responses to either heat or mechanical stimuli in the CFA model (Fig. 4*B*). These data indicate an essential contribution of $Na_v1.7$ to neural activity underlying behavioral hypersensitivity to heat stimuli after inflammation.

Fos induction in dorsal horn neurons by a non-noxious warm stimulus occurs after burn injury in control but not $Na_v1.7$ cKO mice

Activity-dependent expression of Fos in spinal neurons in the pain pathway has been widely used to study the neural circuitry activated by a large variety of noxious stimuli (Hunt et al., 1987; Coggeshall, 2005). Here, we investigated in further detail heat hypersensitivity after burn model injury in control and $Na_v1.7$ cKO mice, using Fos induction in the dorsal horn as a readout. Specifically, we asked whether normally non-noxious warm stimuli activate spinal laminae I-II pain circuits in mice with burn model injury, and whether this effect might be mitigated by deletion of $Na_v1.7$.

In control mice without burn model injury, immersion of one hindpaw into a 40°C water bath did not induce Fos expression in spinal neurons (Fig. 5*A*,*B*,*I*). This finding is similar to an earlier

←

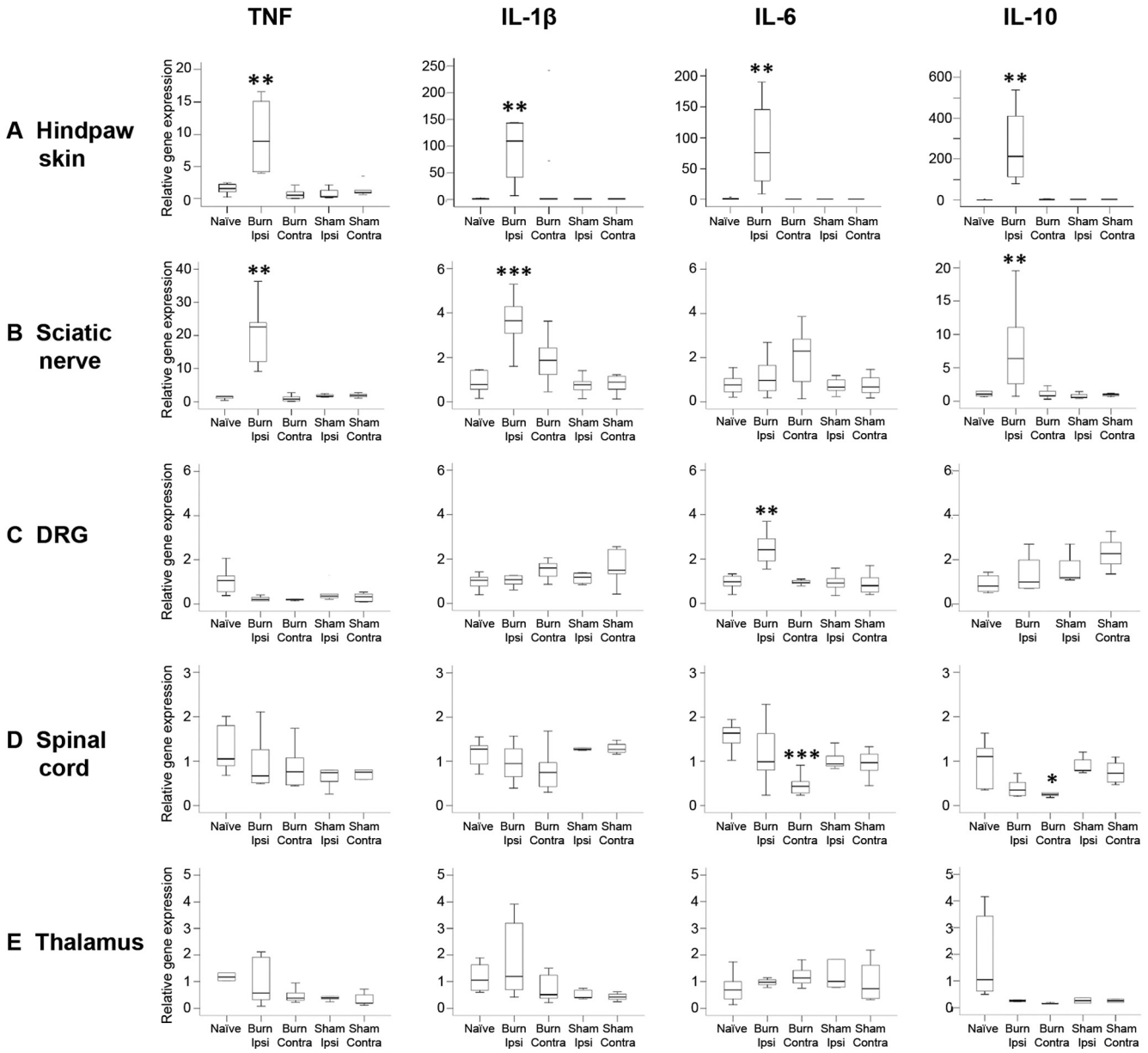

Figure 3. Cytokine gene regulation along the pain–sensory neuraxis at 24 h following burn model injury. The pro-inflammatory cytokines TNF, IL-1β, and IL-6, and the anti-inflammatory cytokine IL-10 were tracked by qRT-PCR in various tissues. The qRT-PCR data are illustrated as box-and-whisker plots giving the median, the upper 75% and lower 25% percentiles, and the minimum and maximum values. ***A***, The expression of TNF ($p < 0.01$), IL-1β ($p < 0.01$), IL-6 ($p < 0.01$), and IL-10 ($p < 0.01$) were increased in the hindpaw skin of burn model animals on the ipsilateral side compared with controls. ***B***, The expression of TNF ($p < 0.01$), IL-1β ($p < 0.001$), and IL-10 ($p < 0.01$) was increased in the sciatic nerves of burn model animals on the ipsilateral side compared with controls. ***C***, The expression of IL-6 ($p < 0.01$) was increased in lumbar DRGs of burn model animals on the ipsilateral side compared with controls. ***D***, The expression of IL-6 ($p < 0.001$) and IL-10 ($p < 0.05$) were decreased in lumbar spinal cord of burn model animals on the contralateral side compared with controls. ***E***, Gene expression of the investigated cytokines did not change in the thalamus. *$p < 0.05$; **$p < 0.01$; ***$p < 0.001$.

study that reported radiant heating to 40°C is also insufficient for Fos induction (Hunt et al., 1987), and is consistent with a 40°C stimulus being non-noxious. However, in mice that had undergone burn model injury 7 d previously, immersion of the injured hindpaw in 40°C water resulted in a significant induction of Fos in the superficial dorsal horn (Fig. 5*C*,*D*,*I*). We interpret this result to represent a functional anatomical correlate of burn-induced heat allodynia.

In $Na_v1.7$ cKO mice with prior burn model injury, the 40°C stimulus did not induce Fos in dorsal horn neurons compared with non-stimulated controls (Fig. 5*E*,*F*,*I*). This finding recapitulates the loss of behavioral heat hypersensitivity in $Na_v1.7$ cKO mice. Finally, we tested $Na_v1.8$ KO animals in the same paradigm. As in control mice with a normal complement of sodium channels, $Na_v1.8$ KO mice with prior burn model injury underwent a significant induction of Fos in the superficial dorsal horn upon exposure to the warm 40°C stimulus (Fig. 5*G–I*), in agreement with their intact responses in behavioral testing. These results emphasize the critical involvement of $Na_v1.7$ in heat hypersensitivity, in this case at the level of primary afferent activity that gives rise to plasticity of gene expression in the postsynaptic neurons of the pain pathway.

To complement these experiments, we used a separate cohort of mice to examine the effect of a normally non-noxious mechan-

ical stimulus on spinal Fos expression after burn injury. In rats, walking on a rotating beam induces Fos expression in spinal neurons that respond to non-noxious stimuli, including those in laminae III-VII and the protein kinase Cγ interneurons of the ventral portion of inner lamina II (lamina IIiv), but not in lamina I or outer lamina II (lamina IIo), regions that contain neurons predominantly responsive to noxious stimuli (Jasmin et al., 1994; Neumann et al., 2008). In control mice without burn injury, we found a similar pattern of Fos expression after walking on the rotating beam, including very few Fos-immunoreactive profiles in laminae I-II, suggesting that this stimulus is indeed non-noxious (Fig. 5*J*,*K*,*R*). In contrast, wild-type mice that had undergone burn model injury 7 d previously displayed, in addition to the expected labeling in deep dorsal horn, a strong induction of Fos in laminae I-II ipsilateral to the burn. This superficial labeling represented a significant induction compared with both nonburned animals and to the contralateral side (Fig. 5*L*,*M*,*R*). Touch-evoked Fos induction in laminae I-II neurons has been shown previously in the setting of CFA inflammation (Ma and Woolf, 1996), and here we extend these observations to include that a natural self-driven stimulus (walking) can also induce activity-dependent gene expression changes in superficial dorsal horn neurons in the setting of burn injury.

In $Na_v1.7$ cKO mice with prior burn model injury, walking on the rotating beam elicited Fos induction in laminae I-II ipsilateral to the burn, as well as in deeper laminae on both sides of the spinal cord, similar to wild-type mice (Fig. 5*N*,*O*,*R*). The same pattern of Fos induction was also observed in $Na_v1.8$ KO mice that had undergone burn model injury (Fig. 5*P*–*R*). Thus, these results parallel the findings of our behavioral assays, in which burn injury-induced mechanical hypersensitivity was present in mice of all genotypes tested, and underscore the modality-specific effect of cKO of the $Na_v1.7$ channel.

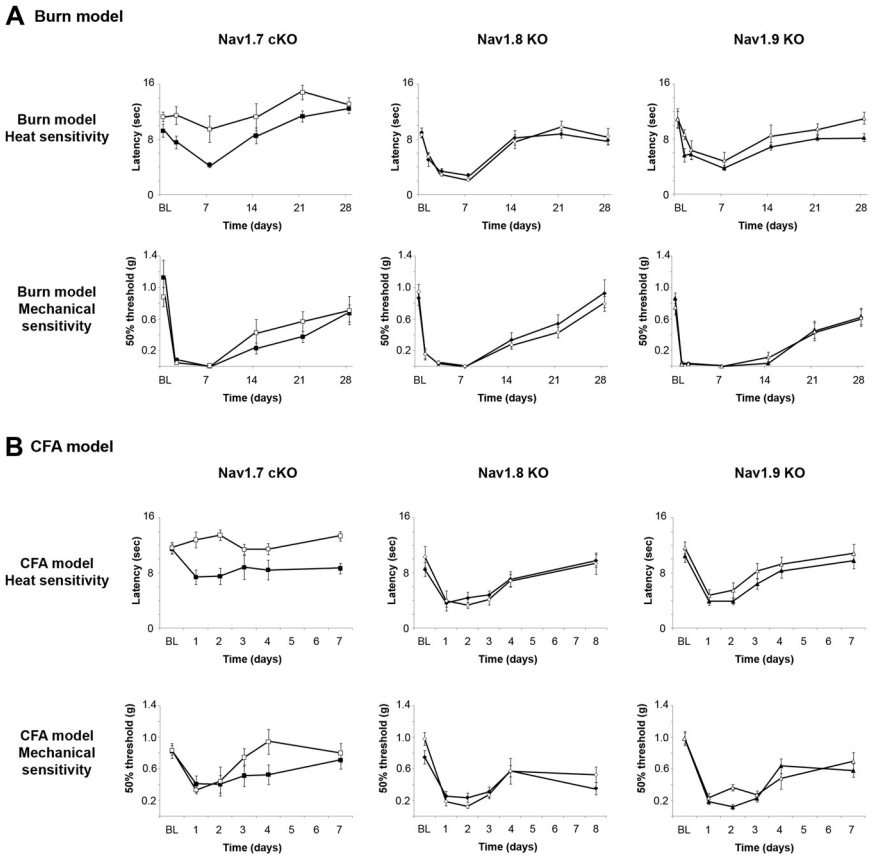

Figure 4. $Na_v1.7$ cKO mice do not become hypersensitive to heat stimuli in the burn model or the CFA model of inflammatory pain. Filled symbols indicate control littermates, open symbols indicate $Na_v1.7$ cKO mice (squares), $Na_v1.8$ KO mice (diamonds), or $Na_v1.9$ KO mice (triangles). ***A***, $Na_v1.7$ cKO mice do not develop reduced withdrawal thresholds to heat stimuli after burn model injury, unlike control littermates (repeated-measures ANOVA, $p < 0.05$; $n = 16$ $Na_v1.7$ cKO mice, 14 control [floxed] littermates). However, reduced withdrawal thresholds to mechanical stimuli develop in $Na_v1.7$ cKO mice, indistinguishably from controls. $Na_v1.8$ KO and $Na_v1.9$ KO have normal pain-like responses to both heat and mechanical modalities after burn model injury ($n = 9$ $Na_v1.8$ KO, 8 $Na_v1.8$ wild type; $n = 7$ $Na_v1.9$ KO, 7 $Na_v1.9$ wild type). ***B***, Similar results were found in the CFA model of inflammatory pain. $Na_v1.7$ cKO mice do not develop reduced withdrawal thresholds to heat stimuli in the CFA model, unlike control littermates (repeated-measures ANOVA, $p < 0.05$; $n = 8$ $Na_v1.7$ cKO mice, 7 control [floxed] littermates). However, reduced withdrawal thresholds to mechanical stimuli develop in $Na_v1.7$ cKO mice, indistinguishably from controls. $Na_v1.8$ KO and $Na_v1.9$ KO have normal pain-like responses to both heat and mechanical modalities in the CFA model ($n = 8$ $Na_v1.8$ KO, 7 $Na_v1.8$ wild type; $n = 9$ $Na_v1.9$ KO, 9 $Na_v1.9$ wild type).

Burn model injury induces altered $Na_v1.7$ properties in DRG neurons

To explore the mechanistic basis for how $Na_v1.7$ may be involved in the development of heat hypersensitivity, we analyzed TTX-S currents in sensory neurons from mice with burn model injury or sham treatment. Specifically, we recorded from neurons labeled by Cre-dependent expression of the tdTomato red fluorescent protein from control mice bearing the genotype [$Na_v1.8^{Cre/+}$; $Na_v1.7^{+/+}$; $Rosa26^{tdTomato/tdTomato}$] or $Na_v1.7$ cKO mice bearing the genotype [$Na_v1.8^{Cre/+}$; $Na_v1.7^{loxP/loxP}$; $Rosa26^{tdTomato/tdTomato}$]. This strategy enabled us to compare a uniform population of sensory neurons in both groups of mice, namely the $Na_v1.8$-Cre-expressing population, whose neurochemical characteristics have been described (Shields et al., 2012). Furthermore, it allowed us to be sure that neurons recorded from $Na_v1.7$ cKO mice were truly $Na_v1.7$-negative (some DRG neurons may still express $Na_v1.7$ due to the cKO strategy). Although we restricted our recordings to tdTomato-expressing L4–L6 DRG neurons ipsilateral to the burn injury (or sham treatment), we could not ensure every recorded neuron innervated the plantar surface of the hindpaw. Any electrophysiological changes must therefore be considered to underestimate the effects of burn injury on DRG neurons, due to effect-size dilution from potential pooling of data from injured and noninjured neurons from the same ganglia.

To eliminate the influence of driving force on current density comparison, TTX-S currents at −20 mV and $Na_v1.8$ currents at 0 mV were used for statistical analysis of current density. In control mice, burn injury increases TTX-S current density (burn: 968 ± 75 pA/pF, $n = 23$; $p < 0.05$ vs sham: 773 ± 56 pA/pF, $n = 28$) (Fig. 6*A*,*D*), whereas no significant change was observed after burn injury for $Na_v1.8$ current density (burn: 92 ± 10 pA/pF, $n = 23$; $p > 0.05$ vs sham: 71 ± 9 pA/pF, $n = 28$) (Fig. 6*A*,*C*). The increase in TTX-S current density could be due to increased channel density in the plasma membrane, although other mech-

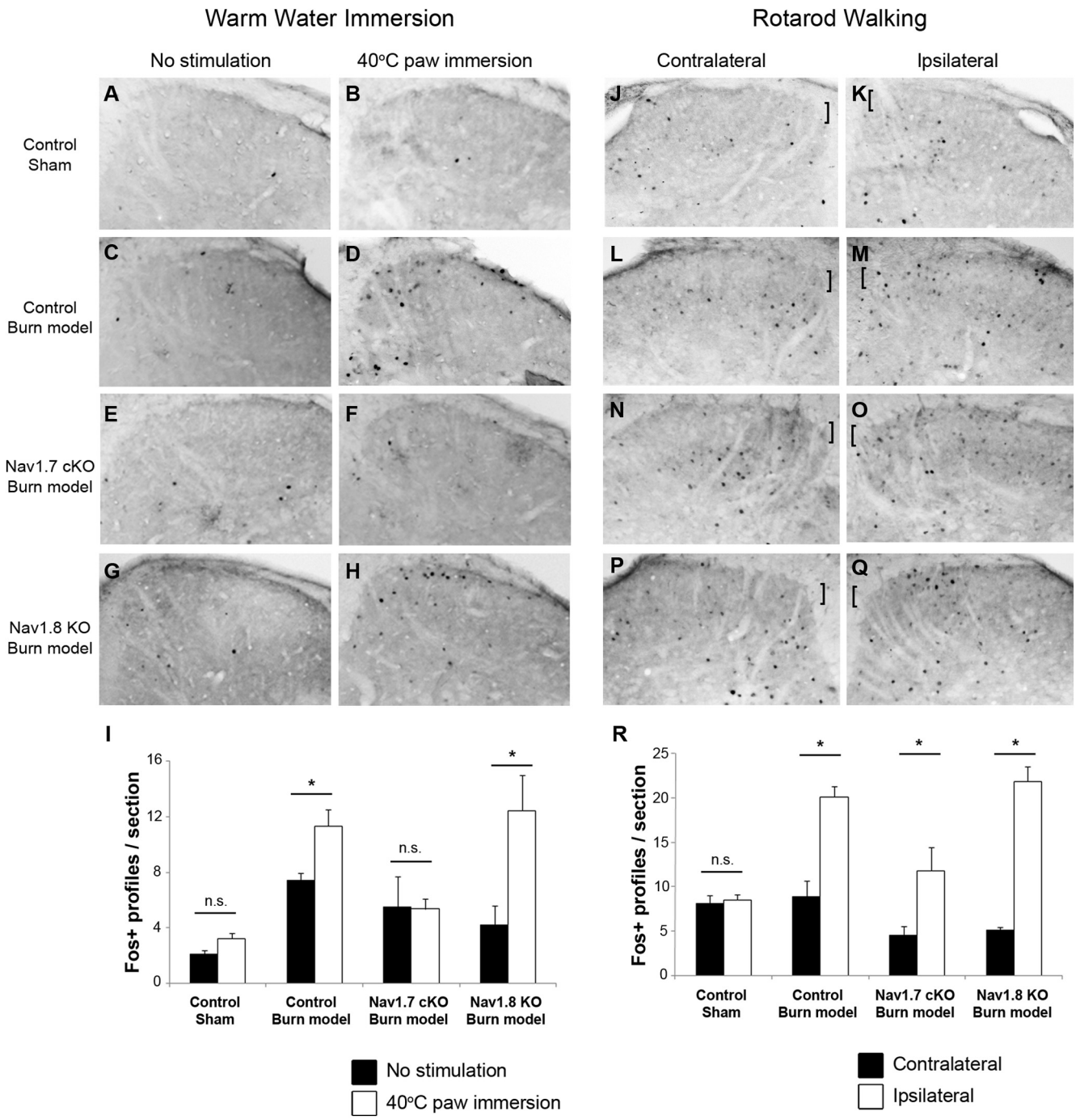

Figure 5. Fos induction in dorsal horn neurons by a non-noxious warm stimulus occurs after burn injury in control and $Na_v1.8$ KO mice, but not $Na_v1.7$ cKO mice. ***A–H***, Representative photomicrographs of spinal cord dorsal horn tissue from sham-treated or burn model mice showing Fos-positive profiles under control conditions (no stimulation, ***A***, ***C***, ***E***, ***G***) or after immersion of the affected hindpaw in a 40°C water bath (***B***, ***D***, ***F***, ***H***). Genotypes and treatment groups are indicated on the left. ***I***, Quantification of Fos-positive profiles per section. The warm stimulus did not induce Fos in sham-treated mice, thus we argue that 40°C is not normally a noxious stimulus in uninjured mice. However, in mice that had previously undergone burn model injury, immersion of the paw in 40°C water induces Fos in spinal laminae I-II. This effect is still present in mice lacking $Na_v1.8$, but is abolished in $Na_v1.7$ cKO mice. ***J–Q***, Representative images of spinal cord dorsal horn tissue from sham-treated or burn model mice showing Fos-positive profiles after walking on a rotating beam (contralateral to sham/burn-injured hindpaw, ***J***, ***L***, ***N***, ***P***; ipsilateral to sham/burn-injured hindpaw, ***K***, ***M***, ***O***, ***Q***). Genotypes and treatment groups are indicated on the left. ***R***, Quantification of Fos-positive profiles per section. Walking on a rotating beam induced Fos expression only in lamina III and deeper laminae in sham-treated mice and on the side contralateral to burn injury, and is thus considered a non-noxious mechanical stimulus. However, in mice that had previously undergone burn model injury, walking on the rotating beam induces Fos in laminae I-II of the ipsilateral dorsal horn as well (denoted by brackets). This is true in mice of all genotypes tested. *$p < 0.05$.

anisms at the level of single channels (increased probability of opening or increased conductance per channel) may also make a contribution.

DRG neurons from $Na_v1.7$ cKO mice produced smaller TTX-S currents, with current densities ~61% of that in control mice ($Na_v1.7$ cKO sham: 474 ± 74 pA/pF, $n = 14$) (Fig. 6*A*,*E*), probably due to the absence of $Na_v1.7$ channels. Burn model injury in $Na_v1.7$ cKO mice did not affect current density of TTX-S channels ($Na_v1.7$ cKO burn: 529 ± 77 pA/pF, $n = 18$; $p > 0.05$ vs $Na_v1.7$ cKO sham) (Fig. 6*E*,*H*), nor $Na_v1.8$ current density

($Na_v1.7$ cKO burn: 114 ± 12 pA/pF, n = 18; $p > 0.05$ vs $Na_v1.7$ cKO sham: 87 ± 11 pA/pF, n = 14) (Fig. 6*E*,*G*).

In $Na_v1.7$ cKO DRG neurons, burn model injury has no effect on the kinetics of activation or fast-inactivation of TTX-S or $Na_v1.8$ channels (Fig. 6*F*, Tables 2 and 3). However, in DRG neurons from mice with the control genotype, burn model injury causes a small but significant hyperpolarizing shift in activation of TTX-S currents ($V_{1/2}$ burn: −35.1 ± 1.1 mV, n = 15; $p < 0.05$ vs $V_{1/2}$ sham: −32.1 ± 0.6 mV, n = 20) (Fig. 6*B*; Table 2). No differences were observed in voltage dependence of fast-inactivation between neurons from burn-injured or sham-treated mice from either genotype (Table 3).

Discussion

In this study, we have established and thoroughly characterized a model of burn injury-induced pain in wild-type and transgenic mice, which we hope will provide a platform for preclinical investigation of mechanisms and treatments for burn-related pain. Using this model, our behavioral, functional-anatomical, and electrophysiological experiments have allowed us to demonstrate that, among the sodium channel isoforms preferentially expressed in the peripheral nervous system, $Na_v1.7$ is an essential contributor to burn-induced hypersensitivity to heat stimuli.

Mice with a cKO of $Na_v1.7$ do not display signs of hypersensitivity to heat stimuli after undergoing burn model injury or in the CFA model, indicating that $Na_v1.7$ is necessary for this particular aspect of pain. To be more precise, activity of $Na_v1.7$ within the subset of sensory neurons that expresses $Na_v1.8$ seems to be required for the observed phenotypes. $Na_v1.8$ and $Na_v1.9$ seem not to be indispensible in the same way, at least not individually, since mice lacking either one of these channels responded similarly to wild-type mice in our assays. It is interesting to note that, within the same subset of neurons (the $Na_v1.8$ population), the absence of $Na_v1.7$ versus the absence of $Na_v1.8$ results in a differential phenotype. This important result rules out the possibility that these two sodium channel isoforms can directly substitute for each other, and underscores the fact that the unique biophysical signatures of the different members of the VGSC family ultimately correspond to distinct functions in the whole animal.

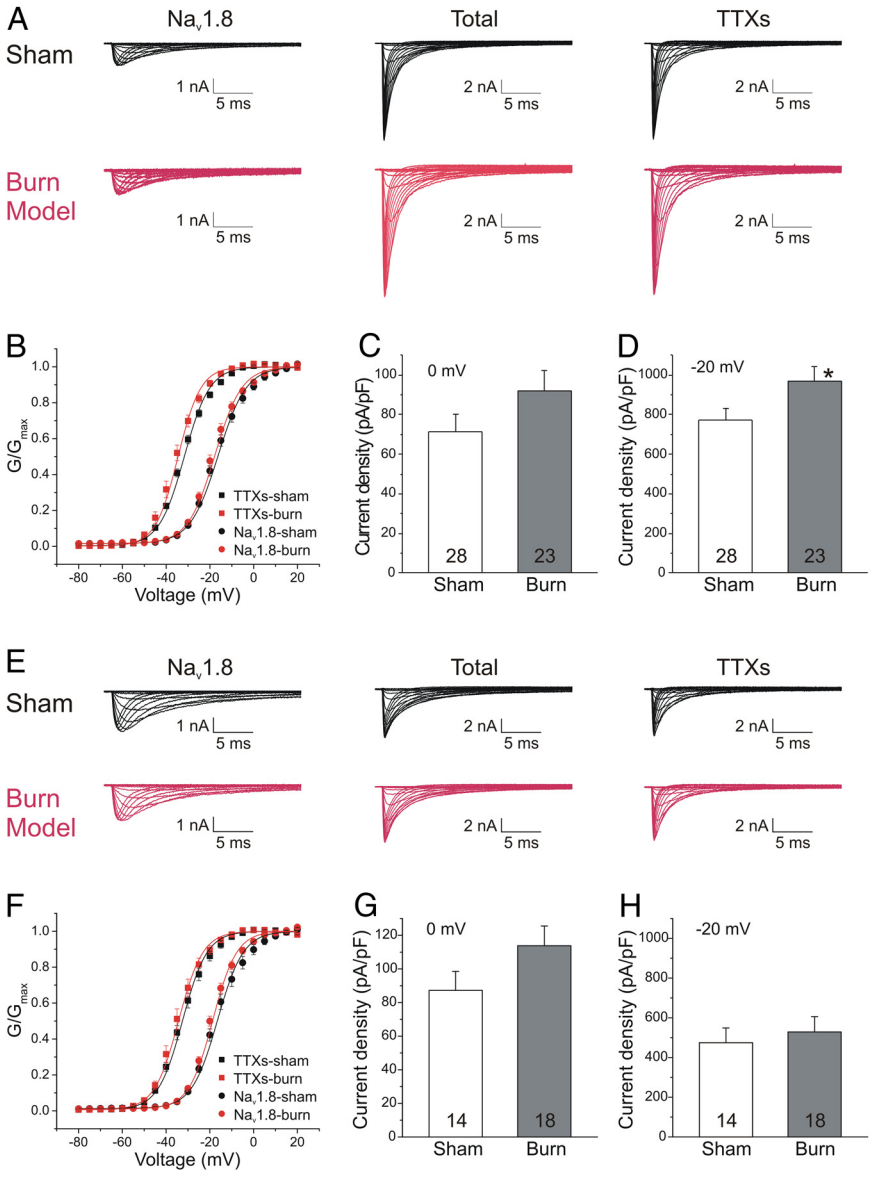

Figure 6. Burn model injury increases TTX-S current density and enhances activation of TTX-S channels in DRG neurons of wild-type but not $Na_v1.7$ cKO mice. ***A–D***, Control mice; ***E–H***, $Na_v1.7$ cKO mice. ***A***, Representative voltage-dependent inward currents from $Na_v1.8$ channels (left), total sodium channels (middle), and TTX-S channels (right, obtained by subtracting $Na_v1.8$ currents from total sodium currents) in DRG neurons isolated from control mice that underwent sham procedure (top) or burn model injury (bottom). ***B***, Burn model injury has no effect on $Na_v1.8$ activation, but shifts the activation curve of TTX-S channels by ~−3 mV in DRG neurons from control mice. ***C***, There is no significant difference in the mean values of $Na_v1.8$ current density in DRG neurons isolated from control mice with sham treatment or burn model injury. ***D***, DRG neurons isolated from mice that had undergone burn model injury produce larger TTX-S currents than neurons from sham-treated animals. ***E***, Representative voltage-dependent inward currents of $Na_v1.8$ channels (left), total sodium channels (middle), and TTX-S channels (right, obtained by subtracting $Na_v1.8$ currents from total sodium currents) in DRG neurons isolated from $Na_v1.7$ cKO mice that underwent sham procedure (top) or burn model injury (bottom). ***F***, Burn model injury has no effect on voltage-dependent activation of $Na_v1.8$ or TTX-S channels in DRG neurons from $Na_v1.7$ cKO mice. ***G***, There is no significant difference in the mean values of $Na_v1.8$ current density in DRG neurons isolated from $Na_v1.7$ cKO mice with sham treatment or burn model injury. ***H***, There is no significant difference in TTX-S current density between DRG neurons from sham-treated or burn model $Na_v1.7$ cKO mice. *$p < 0.05$.

The electrophysiological properties of $Na_v1.7$ were changed significantly in two ways by burn injury. First, we detected an increased density of TTX-S current attributable to $Na_v1.7$ in DRG neurons derived from mice that had undergone burn model injury. Second, there is a small but statistically significant hyperpolarizing shift in $Na_v1.7$ activation in DRG neurons derived from burn model mice compared with sham-treated animals, possibly due to phosphorylation of the channel by ERK1/2 (e.g., residues T531, S535, S608, and S712 in the first intracellular loop) (Stamboulian et al., 2010). These two electrophysiological alterations suggest that more $Na_v1.7$ channels are available for activation at the membrane, and also that each channel can be recruited by

Table 2. Voltage-dependent activation of Nav1.8 and TTX-S currents in small DRG neurons

	Nav1.8			TTX-S		
Channels	$V_{1/2,act}$	k	n	$V_{1/2,act}$	k	n
1.7-cKO						
Sham	−16.5 ± 1.3	−6.78 ± 0.46	10	−32.5 ± 1.1	−6.10 ± 0.26	13
Burn	−19.0 ± 0.8	−5.87 ± 0.21	15	−34.5 ± 1.3	−5.65 ± 0.40	12
1.7-control						
Sham	−16.8 ± 1.0	−7.01 ± 0.37	12	−32.1 ± 0.6	−6.20 ± 0.23	20
Burn	−18.5 ± 0.9	−6.47 ± 0.34	15	−35.1 ± 1.1*	−5.54 ± 0.28	15

*$p < 0.05$ burn versus sham.

Table 3. Steady-state fast inactivation of voltage-dependent sodium currents in small DRG neurons

	Double Boltzmann fitting							Single Boltzmann fitting			
	Phase 1		Phase 2								
Groups	$V_{1/2,fast1}$	k_1	$V_{1/2,fast2}$	k_2	R_{resist} (%)	Fraction	n	$V_{1/2,fast}$	k	R_{resist} (%)	n
1.7-cKO											
Sham	−86.1 ± 1.9	7.90 ± 0.40	−45.6 ± 1.1	3.70 ± 0.33	1.4 ± 0.6	0.82 ± 0.05	8				
Burn	−87.8 ± 1.0	8.01 ± 0.88	−46.6 ± 0.9	3.93 ± 0.24	0.8 ± 0.1	0.78 ± 0.06	11				
1.7-control											
Sham	−87.8 ± 1.6	6.39 ± 0.41	−45.5 ± 1.5	3.95 ± 0.47	0.6 ± 0.1	0.93 ± 0.01	6	−92.0 ± 1.4	9.01 ± 0.24	1.2 ± 0.4	9
Burn	−87.7 ± 1.7	6.16 ± 0.28	−45.6 ± 1.2	3.97 ± 0.42	0.2 ± 0.1*	0.98 ± 0.01	7	−89.3 ± 1.5	8.87 ± 0.39	1.0 ± 0.3	10

*$p < 0.05$ burn versus sham.

smaller displacements of membrane voltage, for example, small currents due to weak activation of transient receptor potentials (TRPs) or other transducer channels. $Na_v1.7$'s role in electrogenesis in DRG neurons is thought to be to sense such transducer currents and amplify them into a signal that activates other VGSCs and that is capable of triggering an action potential (Cummins et al., 1998; Rush et al., 2007). Thus, any hyperpolarizing shift in $Na_v1.7$ activation will reduce the amount of transducer current necessary to generate firing activity, effectively lowering the neuron's threshold, as has been demonstrated in DRG neurons expressing mutant $Na_v1.7$ channels with hyperpolarized activation (Dib-Hajj et al., 2005; Rush et al., 2006; Han et al., 2009).

The results of our Fos study provide a functional anatomical readout, at the level of activity-dependent changes in postsynaptic gene expression, of hypersensitivity to a normally non-noxious warm stimulus after burn model injury. The nature of the stimulus clearly frames our observation as an example of heat allodynia (defined as "pain due to a stimulus that does not normally provoke pain") rather than heat hyperalgesia ("increased pain from a stimulus that normally provokes pain"; Cervero and Laird, 1996; Loeser and Treede, 2008)). It is, to our knowledge, the first reported example of Fos expression in spinal dorsal horn neurons evoked by a non-noxious heat stimulus (Coggeshall, 2005). We postulate that a peripheral sensitization mechanism is likely responsible in this case, wherein $Na_v1.7$- and $Na_v1.8$-co-expressing heat-sensitive primary afferents are more readily activated after burn model injury, and therefore a mild warm stimulus gains access to pain circuitry in the spinal cord, resulting in heat allodynia.

An interesting question is whether the heat-sensitive neurons responsible for heat hypersensitivity are high-threshold (noxious heat-sensing nociceptors) or low-threshold (warm-sensitive) neurons. In one scenario, warm-sensitive neurons affected by hindpaw burn would become hyperexcitable due to changes in the electrophysiological properties of $Na_v1.7$ and would produce more action potentials in response to their adequate stimulus (e.g., 40°C). It is not entirely clear in this case how warm-sensitive afferents would gain the ability to communicate via heat-pain pathways in the spinal cord, although a system analogous to the disinhibition demonstrated in touch-pain for the mechanical modality (Yaksh, 1989; Sivilotti and Woolf, 1994; Torsney and MacDermott, 2006; Miraucourt et al., 2009) could be involved. This would require warm-sensitive neurons to be prewired to second-order pain-sensitive neurons, and additionally invokes changes in spinal interneurons. Alternatively, within heat nociceptors, small transducer currents generated by marginal activation of TRPV1 at 40°C (Cesare and McNaughton, 1996; Tominaga et al., 1998) that are normally below the threshold for activating VGSCs could become sufficient after burn injury to set off the events leading to action potential generation in the context of $Na_v1.7$'s hyperpolarized activation threshold. The hypothesis that heat nociceptors rather than low-threshold warm-sensitive sensory neurons are the neural substrate for heat allodynia in inflammation models is supported by evidence demonstrating that silencing TRPV1-expressing heat nociceptors completely abolishes behavioral responses to heat in the setting of established CFA-induced inflammatory pain (Cavanaugh et al., 2009).

In contrast to the deficit in heat hypersensitivity observed in $Na_v1.7$ cKO mice, burn- and CFA-induced mechanical hypersensitivity remained intact in each of the three sodium channel mutant mouse lines tested in our assays. Apparently, heat and mechanical sensitization are dissociable and likely controlled by different mechanisms, as suggested by several other studies (Tal and Bennett, 1994; Ali et al., 1996; Mazarío and Basbaum, 2007). However, our behavioral results contradict the findings of Nassar et al. (2004), who reported that sensitization to mechanical stimuli was absent after CFA in the same line of $Na_v1.7$ cKO mice that was used here. Perhaps differences in the methodological details of the testing or in the animals' genetic background due to additional back-crossing generations can explain the differences. Nevertheless, we suggest that our current findings of intact mechanical sensitization in sodium channel-null mutant mice could be explained if the regulation of mechanical pain thresholds involves a complex interplay of redundant mechanisms that is robust to the deletion of a single sodium channel type. Alternatively, mechanical sensitization could be mediated by a different subset of sensory neurons than the

ones affected by our experimental manipulations, such as the $Na_v1.8$-negative population. The $Na_v1.8$-negative DRG neurons include about half of the large-diameter NF200-positive neurons with myelinated axons (Shields et al., 2012) and should be explored in more detail as potential drivers of mechanically evoked pathological pain.

It is important to bear in mind the limitations of the cKO approach we have used in this study. In $Na_v1.7$ cKO mice, $Na_v1.7$ is removed from cells in which $Na_v1.8$ has been expressed (i.e., $Na_v1.8$-Cre-driven cKO). It is likely that $Na_v1.7$ is still present where $Na_v1.8$ is not expressed, potentially in as many as 25% of DRG neurons (Black et al., 1996; Shields et al., 2012), as well as in the sympathetic nervous system (Sangameswaran et al., 1996; Toledo-Aral et al., 1997; Minett et al., 2012). In this context, the finding that mechanical hypersensitivity remains intact in $Na_v1.7$ cKO mice should not be overinterpreted as ruling out the involvement of $Na_v1.7$ in this process as well. That is, it is possible the same proposed mechanism, whereby the voltage dependence of activation of $Na_v1.7$ is shifted in the hyperpolarized direction, causing a drop in neuronal threshold, could be operating in the $Na_v1.8$-negative sensory neurons and contribute to burn-induced mechanical hypersensitivity. However, this is just one candidate mechanism among many, both sodium channel-related and -unrelated. Further study is clearly necessary to elucidate the molecular and cellular basis of burn-induced mechanical hypersensitivity.

Overall, we have demonstrated that the presence of $Na_v1.7$ is a prerequisite for heat hypersensitivity after burn injury. Moreover, our data suggest that circumscribed alterations in the biophysical properties of $Na_v1.7$ have wide-ranging consequences that contribute to the excitability of primary afferent nociceptors and their communication with and ability to induce gene expression changes in higher order neurons along spinal pain pathways, ultimately setting behavioral thresholds to heat stimuli and driving the evolutionarily adaptive behavior of protection of an injured body part. Furthermore, our results serve to narrow down the molecular and cellular candidates responsible for sensing different modalities of pain. We suggest that $Na_v1.7$-blocking drugs currently being developed for erythromelalgia and small-fiber neuropathy may have cross-over potential for controlling pain in burn patients as well.

References

Abbadie C, Bhangoo S, De Koninck Y, Malcangio M, Melik-Parsadaniantz S, White FA (2009) Chemokines and pain mechanisms. Brain Res Rev 60:125–134.

Akopian AN, Souslova V, England S, Okuse K, Ogata N, Ure J, Smith A, Kerr BJ, McMahon SB, Boyce S, Hill R, Stanfa LC, Dickenson AH, Wood JN (1999) The tetrodotoxin-resistant sodium channel SNS has a specialized function in pain pathways. Nat Neurosci 2:541–548.

Ali Z, Meyer RA, Campbell JN (1996) Secondary hyperalgesia to mechanical but not heat stimuli following a capsaicin injection in hairy skin. Pain 68:401–411.

Amaya F, Decosterd I, Samad TA, Plumpton C, Tate S, Mannion RJ, Costigan M, Woolf CJ (2000) Diversity of expression of the sensory neuron-specific TTX-resistant voltage-gated sodium ion channels SNS and SNS2. Mol Cell Neurosci 15:331–342.

Amaya F, Wang H, Costigan M, Allchorne AJ, Hatcher JP, Egerton J, Stean T, Morisset V, Grose D, Gunthorpe MJ, Chessell IP, Tate S, Green PJ, Woolf CJ (2006) The voltage-gated sodium channel Na(v)1.9 is an effector of peripheral inflammatory pain hypersensitivity. J Neurosci 26:12852–12860.

Black JA, Dib-Hajj S, McNabola K, Jeste S, Rizzo MA, Kocsis JD, Waxman SG (1996) Spinal sensory neurons express multiple sodium channel alpha-subunit mRNAs. Brain Res Mol Brain Res 43:117–131.

Blair NT, Bean BP (2002) Roles of tetrodotoxin (TTX)-sensitive Na+ current, TTX-resistant Na+ current, and Ca2+ current in the action potentials of nociceptive sensory neurons. J Neurosci 22:10277–10290.

Bráz JM, Basbaum AI (2009) Triggering genetically expressed transneuronal tracers by peripheral axotomy reveals convergent and segregated sensory neuron-spinal cord connectivity. Neuroscience 163:1220–1232.

Caterina MJ, Leffler A, Malmberg AB, Martin WJ, Trafton J, Petersen-Zeitz KR, Koltzenburg M, Basbaum AI, Julius D (2000) Impaired nociception and pain sensation in mice lacking the capsaicin receptor. Science 288:306–313.

Cavanaugh DJ, Lee H, Lo L, Shields SD, Zylka MJ, Basbaum AI, Anderson DJ (2009) Distinct subsets of unmyelinated primary sensory fibers mediate behavioral responses to noxious thermal and mechanical stimuli. Proc Natl Acad Sci U S A 106:9075–9080.

Cervero F, Laird JM (1996) Mechanisms of touch-evoked pain (allodynia): a new model. Pain 68:13–23.

Cesare P, McNaughton P (1996) A novel heat-activated current in nociceptive neurons and its sensitization by bradykinin. Proc Natl Acad Sci U S A 93:15435–15439.

Chang YW, Tan A, Saab C, Waxman S (2010) Unilateral focal burn injury is followed by long-lasting bilateral allodynia and neuronal hyperexcitability in spinal cord dorsal horn. J Pain 11:119–130.

Chaplan SR, Bach FW, Pogrel JW, Chung JM, Yaksh TL (1994) Quantitative assessment of tactile allodynia in the rat paw. J Neurosci Methods 53:55–63.

Cheng X, Dib-Hajj SD, Tyrrell L, Te Morsche RH, Drenth JP, Waxman SG (2011) Deletion mutation of sodium channel Na(V)1.7 in inherited erythromelalgia: enhanced slow inactivation modulates dorsal root ganglion neuron hyperexcitability. Brain 134:1972–1986.

Choi JS, Cheng X, Foster E, Leffler A, Tyrrell L, Te Morsche RH, Eastman EM, Jansen HJ, Huehne K, Nau C, Dib-Hajj SD, Drenth JP, Waxman SG (2010) Alternative splicing may contribute to time-dependent manifestation of inherited erythromelalgia. Brain 133:1823–1835.

Chomczynski P, Sacchi N (1987) Single-step method of RNA isolation by acid guanidinium thiocyanate-phenol-chloroform extraction. Anal Biochem 162:156–159.

Coggeshall RE (2005) Fos, nociception and the dorsal horn. Prog Neurobiol 77:299–352.

Coull JA, Beggs S, Boudreau D, Boivin D, Tsuda M, Inoue K, Gravel C, Salter MW, De Koninck Y (2005) BDNF from microglia causes the shift in neuronal anion gradient underlying neuropathic pain. Nature 438:1017–1021.

Cummins TR, Waxman SG (1997) Downregulation of tetrodotoxin-resistant sodium currents and upregulation of a rapidly repriming tetrodotoxin-sensitive sodium current in small spinal sensory neurons after nerve injury. J Neurosci 17:3503–3514.

Cummins TR, Howe JR, Waxman SG (1998) Slow closed-state inactivation: a novel mechanism underlying ramp currents in cells expressing the hNE/PN1 sodium channel. J Neurosci 18:9607–9619.

Cummins TR, Dib-Hajj SD, Black JA, Akopian AN, Wood JN, Waxman SG (1999) A novel persistent tetrodotoxin-resistant sodium current in SNS-null and wild-type small primary sensory neurons. J Neurosci 19:RC43.

Cummins TR, Dib-Hajj SD, Waxman SG (2004) Electrophysiological properties of mutant Nav1.7 sodium channels in a painful inherited neuropathy. J Neurosci 24:8232–8236.

Dawes JM, Calvo M, Perkins JR, Paterson KJ, Kiesewetter H, Hobbs C, Kaan TK, Orengo C, Bennett DL, McMahon SB (2011) CXCL5 mediates UVB irradiation-induced pain. Sci Transl Med 3:90ra60.

Devor M, Govrin-Lippmann R, Frank I, Raber P (1985) Proliferation of primary sensory neurons in adult rat dorsal root ganglion and the kinetics of retrograde cell loss after sciatic nerve section. Somatosens Res 3:139–167.

Dib-Hajj SD, Rush AM, Cummins TR, Hisama FM, Novella S, Tyrrell L, Marshall L, Waxman SG (2005) Gain-of-function mutation in Nav1.7 in familial erythromelalgia induces bursting of sensory neurons. Brain 128:1847–1854.

Dib-Hajj SD, Yang Y, Waxman SG (2008) Genetics and molecular pathophysiology of Na(v)1.7-related pain syndromes. Adv Genet 63:85–110.

Dib-Hajj SD, Choi JS, Macala LJ, Tyrrell L, Black JA, Cummins TR, Waxman SG (2009) Transfection of rat or mouse neurons by biolistics or electroporation. Nat Protoc 4:1118–1126.

Dib-Hajj SD, Cummins TR, Black JA, Waxman SG (2010) Sodium channels in normal and pathological pain. Annu Rev Neurosci 33:325–347.

Drenth JP, Waxman SG (2007) Mutations in sodium-channel gene SCN9A

cause a spectrum of human genetic pain disorders. J Clin Invest 117: 3603–3609.

Estacion M, Dib-Hajj SD, Benke PJ, Te Morsche RH, Eastman EM, Macala LJ, Drenth JP, Waxman SG (2008) NaV1.7 gain-of-function mutations as a continuum: A1632E displays physiological changes associated with erythromelalgia and paroxysmal extreme pain disorder mutations and produces symptoms of both disorders. J Neurosci 28:11079–11088.

Han C, Rush AM, Dib-Hajj SD, Li S, Xu Z, Wang Y, Tyrrell L, Wang X, Yang Y, Waxman SG (2006) Sporadic onset of erythermalgia: a gain-of-function mutation in Nav1.7. Ann Neurol 59:553–558.

Han C, Dib-Hajj SD, Lin Z, Li Y, Eastman EM, Tyrrell L, Cao X, Yang Y, Waxman SG (2009) Early- and late-onset inherited erythromelalgia: genotype-phenotype correlation. Brain 132:1711–1722.

Harty TP, Dib-Hajj SD, Tyrrell L, Blackman R, Hisama FM, Rose JB, Waxman SG (2006) Na(V)1.7 mutant A863P in erythromelalgia: effects of altered activation and steady-state inactivation on excitability of nociceptive dorsal root ganglion neurons. J Neurosci 26:12566–12575.

Herzog RI, Cummins TR, Waxman SG (2001) Persistent TTX-resistant Na+ current affects resting potential and response to depolarization in simulated spinal sensory neurons. J Neurophysiol 86:1351–1364.

Hunt SP, Pini A, Evan G (1987) Induction of c-fos-like protein in spinal cord neurons following sensory stimulation. Nature 328:632–634.

Jasmin L, Gogas KR, Ahlgren SC, Levine JD, Basbaum AI (1994) Walking evokes a distinctive pattern of Fos-like immunoreactivity in the caudal brainstem and spinal cord of the rat. Neuroscience 58:275–286.

Kerr BJ, Souslova V, McMahon SB, Wood JN (2001) A role for the TTX-resistant sodium channel Nav 1.8 in NGF-induced hyperalgesia, but not neuropathic pain. Neuroreport 12:3077–3080.

Kleinschnitz C, Brinkhoff J, Zelenka M, Sommer C, Stoll G (2004) The extent of cytokine induction in peripheral nerve lesions depends on the mode of injury and NMDA receptor signaling. J Neuroimmunol 149:77–83.

Lampert A, O'Reilly AO, Dib-Hajj SD, Tyrrell L, Wallace BA, Waxman SG (2008) A pore-blocking hydrophobic motif at the cytoplasmic aperture of the closed-state Nav1.7 channel is disrupted by the erythromelalgia-associated F1449V mutation. J Biol Chem 283:24118–24127.

Ledeboer A, Mahoney JH, Milligan ED, Martin D, Maier SF, Watkins LR (2006) Spinal cord glia and interleukin-1 do not appear to mediate persistent allodynia induced by intramuscular acidic saline in rats. J Pain 7:757–767.

Leo S, D'Hooge R, Meert T (2010) Exploring the role of nociceptor-specific sodium channels in pain transmission using Nav1.8 and Nav1.9 knockout mice. Behav Brain Res 208:149–157.

Loeser JD, Treede RD (2008) The Kyoto protocol of IASP Basic Pain Terminology. Pain 137:473–477.

Ma QP, Woolf CJ (1996) Basal and touch-evoked fos-like immunoreactivity during experimental inflammation in the rat. Pain 67:307–316.

Madisen L, Zwingman TA, Sunkin SM, Oh SW, Zariwala HA, Gu H, Ng LL, Palmiter RD, Hawrylycz MJ, Jones AR, Lein ES, Zeng H (2010) A robust and high-throughput Cre reporting and characterization system for the whole mouse brain. Nat Neurosci 13:133–140.

Mazarío J, Basbaum AI (2007) Contribution of substance P and neurokinin A to the differential injury-induced thermal and mechanical responsiveness of lamina I and V neurons. J Neurosci 27:762–770.

Minett MS, Nassar MA, Clark AK, Passmore G, Dickenson AH, Wang F, Malcangio M, Wood JN (2012) Distinct Nav1.7-dependent pain sensations require different sets of sensory and sympathetic neurons. Nat Commun 3:791.

Miraucourt LS, Moisset X, Dallel R, Voisin DL (2009) Glycine inhibitory dysfunction induces a selectively dynamic, morphine-resistant, and neurokinin 1 receptor- independent mechanical allodynia. J Neurosci 29:2519–2527.

Nagy I, Rang H (1999) Noxious heat activates all capsaicin-sensitive and also a sub-population of capsaicin-insensitive dorsal root ganglion neurons. Neuroscience 88:995–997.

Narita M, Yoshida T, Nakajima M, Narita M, Miyatake M, Takagi T, Yajima Y, Suzuki T (2006) Direct evidence for spinal cord microglia in the development of a neuropathic pain-like state in mice. J Neurochem 97:1337–1348.

Nassar MA, Stirling LC, Forlani G, Baker MD, Matthews EA, Dickenson AH, Wood JN (2004) Nociceptor-specific gene deletion reveals a major role for Nav1.7 (PN1) in acute and inflammatory pain. Proc Natl Acad Sci U S A 101:12706–12711.

Neumann S, Braz JM, Skinner K, Llewellyn-Smith IJ, Basbaum AI (2008) Innocuous, not noxious, input activates PKCgamma interneurons of the spinal dorsal horn via myelinated afferent fibers. J Neurosci 28:7936–7944.

Ostman JA, Nassar MA, Wood JN, Baker MD (2008) GTP up-regulated persistent Na+ current and enhanced nociceptor excitability require NaV1.9. J Physiol 586:1077–1087.

Peck MD (2011) Epidemiology of burns throughout the world. Part I: Distribution and risk factors. Burns 37:1087–1100.

Peters CM, Jimenez-Andrade JM, Jonas BM, Sevcik MA, Koewler NJ, Ghilardi JR, Wong GY, Mantyh PW (2007) Intravenous paclitaxel administration in the rat induces a peripheral sensory neuropathy characterized by macrophage infiltration and injury to sensory neurons and their supporting cells. Exp Neurol 203:42–54.

Pinto V, Derkach VA, Safronov BV (2008) Role of TTX-sensitive and TTX-resistant sodium channels in Adelta- and C-fiber conduction and synaptic transmission. J Neurophysiol 99:617–628.

Polgár E, Hughes DI, Arham AZ, Todd AJ (2005) Loss of neurons from laminas I-III of the spinal dorsal horn is not required for development of tactile allodynia in the spared nerve injury model of neuropathic pain. J Neurosci 25:6658–6666.

Priest BT, Murphy BA, Lindia JA, Diaz C, Abbadie C, Ritter AM, Liberator P, Iyer LM, Kash SF, Kohler MG, Kaczorowski GJ, MacIntyre DE, Martin WJ (2005) Contribution of the tetrodotoxin-resistant voltage-gated sodium channel NaV1.9 to sensory transmission and nociceptive behavior. Proc Natl Acad Sci U S A 102:9382–9387.

Ren K (2010) Emerging role of astroglia in pain hypersensitivity. Jpn Dent Sci Rev 46:86.

Ren K, Dubner R (2010) Interactions between the immune and nervous systems in pain. Nat Med 16:1267–1276.

Renganathan M, Cummins TR, Waxman SG (2001) Contribution of Na(v)1.8 sodium channels to action potential electrogenesis in DRG neurons. J Neurophysiol 86:629–640.

Rush AM, Craner MJ, Kageyama T, Dib-Hajj SD, Waxman SG, Ranscht B (2005) Contactin regulates the current density and axonal expression of tetrodotoxin-resistant but not tetrodotoxin-sensitive sodium channels in DRG neurons. Eur J Neurosci 22:39–49.

Rush AM, Dib-Hajj SD, Liu S, Cummins TR, Black JA, Waxman SG (2006) A single sodium channel mutation produces hyper- or hypoexcitability in different types of neurons. Proc Natl Acad Sci U S A 103:8245–8250.

Rush AM, Cummins TR, Waxman SG (2007) Multiple sodium channels and their roles in electrogenesis within dorsal root ganglion neurons. J Physiol 579:1–14.

Sangameswaran L, Delgado SG, Fish LM, Koch BD, Jakeman LB, Stewart GR, Sze P, Hunter JC, Eglen RM, Herman RC (1996) Structure and function of a novel voltage-gated, tetrodotoxin-resistant sodium channel specific to sensory neurons. J Biol Chem 271:5953–5956.

Scholz J, Woolf CJ (2007) The neuropathic pain triad: neurons, immune cells and glia. Nat Neurosci 10:1361–1368.

Seijffers R, Allchorne AJ, Woolf CJ (2006) The transcription factor ATF-3 promotes neurite outgrowth. Mol Cell Neurosci 32:143–154.

Shields SD, Mazario J, Skinner K, Basbaum AI (2007) Anatomical and functional analysis of aquaporin 1, a water channel in primary afferent neurons. Pain 131:8–20.

Shields SD, Ahn HS, Yang Y, Han C, Seal RP, Wood JN, Waxman SG, Dib-Hajj SD (2012) $Na_v1.8$ expression is not restricted to nociceptors in mouse peripheral nervous system. Pain. Advance online publication. Retrieved July 16, 2012. PMID: 22703890.

Sivilotti L, Woolf CJ (1994) The contribution of GABAA and glycine receptors to central sensitization: disinhibition and touch-evoked allodynia in the spinal cord. J Neurophysiol 72:169–179.

Stamboulian S, Choi JS, Ahn HS, Chang YW, Tyrrell L, Black JA, Waxman SG, Dib-Hajj SD (2010) ERK1/2 mitogen-activated protein kinase phosphorylates sodium channel Na(v)1.7 and alters its gating properties. J Neurosci 30:1637–1647.

Sweitzer SM, Colburn RW, Rutkowski M, DeLeo JA (1999) Acute peripheral inflammation induces moderate glial activation and spinal IL-1beta expression that correlates with pain behavior in the rat. Brain Res 829:209–221.

Swett JE, Torigoe Y, Elie VR, Bourassa CM, Miller PG (1991) Sensory neurons of the rat sciatic nerve. Exp Neurol 114:82–103.

Takahashi Y, Nakajima Y, Sakamoto T (1994) Dermatome mapping in the rat hindlimb by electrical stimulation of the spinal nerves. Neurosci Lett 168:85–88.

Tal M, Bennett GJ (1994) Neuropathic pain sensations are differentially sensitive to dextrorphan. Neuroreport 5:1438–1440.

Tate S, Benn S, Hick C, Trezise D, John V, Mannion RJ, Costigan M, Plumpton C, Grose D, Gladwell Z, Kendall G, Dale K, Bountra C, Woolf CJ (1998) Two sodium channels contribute to the TTX-R sodium current in primary sensory neurons. Nat Neurosci 1:653–655.

Thacker MA, Clark AK, Bishop T, Grist J, Yip PK, Moon LD, Thompson SW, Marchand F, McMahon SB (2009) CCL2 is a key mediator of microglia activation in neuropathic pain states. Eur J Pain 13:263–272.

Toledo-Aral JJ, Moss BL, He ZJ, Koszowski AG, Whisenand T, Levinson SR, Wolf JJ, Silos-Santiago I, Halegoua S, Mandel G (1997) Identification of PN1, a predominant voltage-dependent sodium channel expressed principally in peripheral neurons. Proc Natl Acad Sci U S A 94:1527–1532.

Tominaga M, Caterina MJ, Malmberg AB, Rosen TA, Gilbert H, Skinner K, Raumann BE, Basbaum AI, Julius D (1998) The cloned capsaicin receptor integrates multiple pain-producing stimuli. Neuron 21:531–543.

Torsney C, MacDermott AB (2006) Disinhibition opens the gate to pathological pain signaling in superficial neurokinin 1 receptor-expressing neurons in rat spinal cord. J Neurosci 26:1833–1843.

Tsuda M, Shigemoto-Mogami Y, Koizumi S, Mizokoshi A, Kohsaka S, Salter MW, Inoue K (2003) P2X4 receptors induced in spinal microglia gate tactile allodynia after nerve injury. Nature 424:778–783.

Tsuda M, Inoue K, Salter MW (2005) Neuropathic pain and spinal microglia: a big problem from molecules in "small" glia. Trends Neurosci 28:101–107.

Tsujino H, Kondo E, Fukuoka T, Dai Y, Tokunaga A, Miki K, Yonenobu K, Ochi T, Noguchi K (2000) Activating transcription factor 3 (ATF3) induction by axotomy in sensory and motoneurons: A novel neuronal marker of nerve injury. Mol Cell Neurosci 15:170–182.

Tsuzuki K, Kondo E, Fukuoka T, Yi D, Tsujino H, Sakagami M, Noguchi K (2001) Differential regulation of P2X(3) mRNA expression by peripheral nerve injury in intact and injured neurons in the rat sensory ganglia. Pain 91:351–360.

Uçeyler N, Sommer C (2008) Cytokine regulation in animal models of neuropathic pain and in human diseases. Neurosci Lett 437:194–198.

Uçeyler N, Tscharke A, Sommer C (2007) Early cytokine expression in mouse sciatic nerve after chronic constriction nerve injury depends on calpain. Brain Behav Immun 21:553–560.

Uçeyler N, Tscharke A, Sommer C (2008) Early cytokine gene expression in mouse CNS after peripheral nerve lesion. Neurosci Lett 436:259–264.

White FA, Jung H, Miller RJ (2007) Chemokines and the pathophysiology of neuropathic pain. Proc Natl Acad Sci U S A 104:20151–20158.

Yaksh TL (1989) Behavioral and autonomic correlates of the tactile evoked allodynia produced by spinal glycine inhibition: effects of modulatory receptor systems and excitatory amino acid antagonists. Pain 37:111–123.

Yang Y, Wang Y, Li S, Xu Z, Li H, Ma L, Fan J, Bu D, Liu B, Fan Z, Wu G, Jin J, Ding B, Zhu X, Shen Y (2004) Mutations in SCN9A, encoding a sodium channel alpha subunit, in patients with primary erythermalgia. J Med Genet 41:171–174.